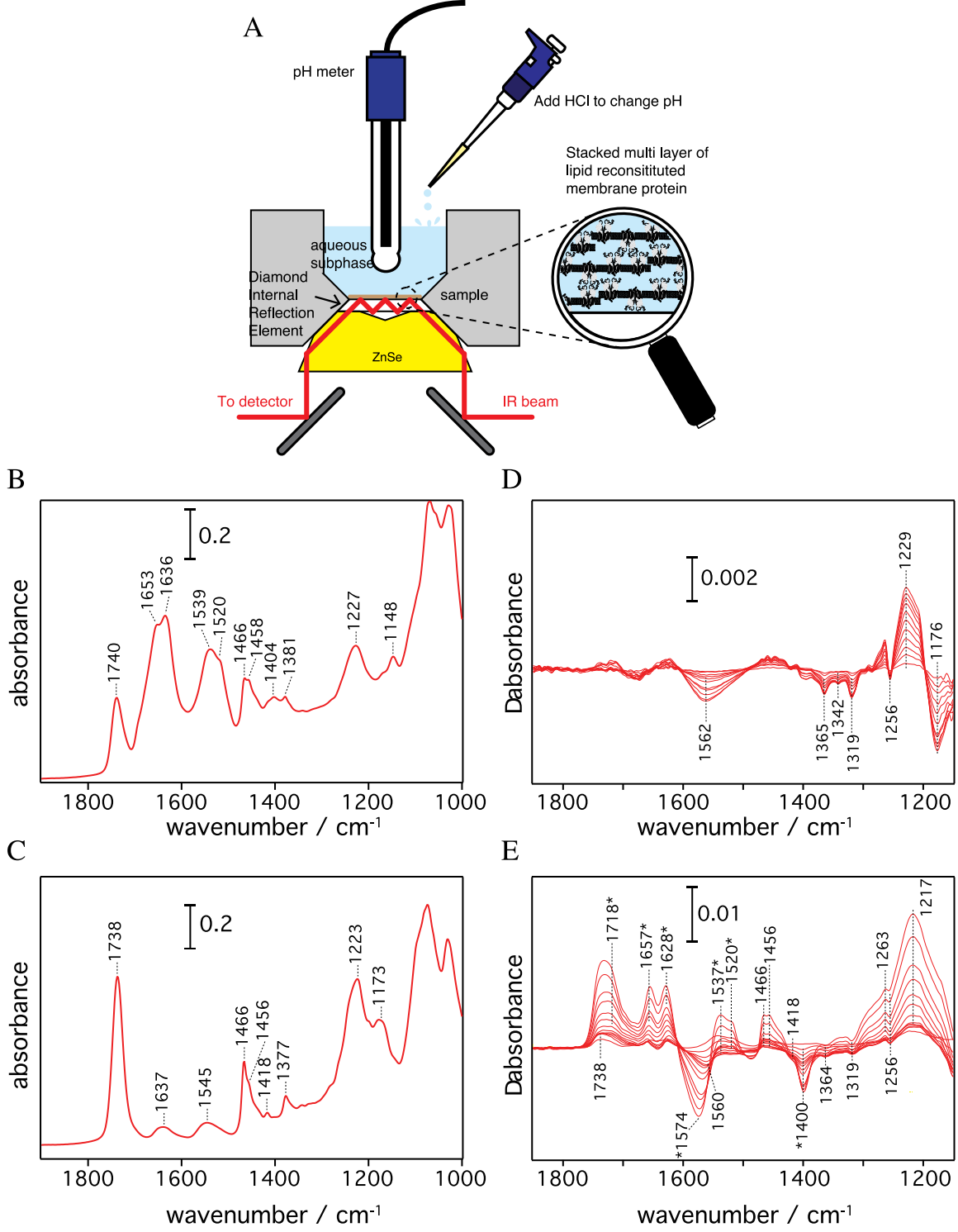

Figure S1. Schematic drawing of the experimental setup of the pH titration ATR-FTIR difference spectroscopy. Multi layers of the lipid reconstituted GLIC stuck on the vicinity of the reflection surface of the IRE. The buffer solution was overlaid on the sample and its pH was changed by adding small aliquots of a 1 M HCl solution. The pH of the buffer solution was monitored by the mounted pH meter in the ATR optical cell. (B)-(D) The ATR FTIR spectra of (B) semi-dried GLIC sample reconstituted in the POPE/POPG lipid, and (C) the POPE/POPG lipid. The pH-induced different FTIR spectra of (D) the buffer solution containing 150 mM NaCl, 20 mM HEPES, and 20 mM MES, and (E) the lipid reconstituted GLIC in the same solution as (D).

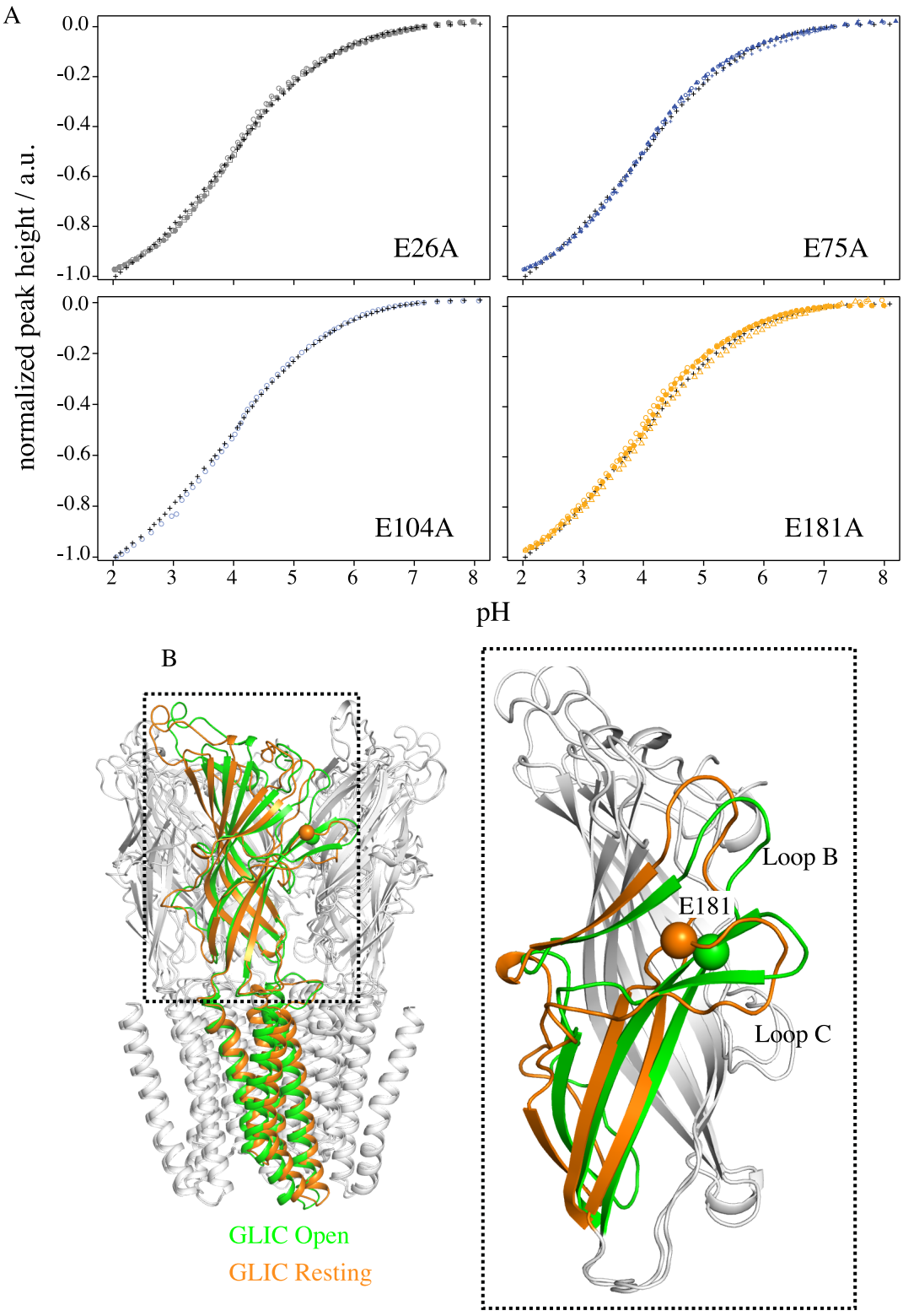

Figure S2. (A) The pH titration curves of E26A, E75A, E104A and E181A derived from the normalized intensities of the carboxylate band at 1400 cm-1. For each mutant, data sets from different experiments are represented with different markers, with titration curves of the wild-type (+) are presented for comparison. (B) Superimposition of GLIC resting/closed form (orange) and GLIC activated/open form (green) to highlight the conformational change of Loop B and loop C during the channel activation. The Cα atom of E181 in both forms are shown as spheres.

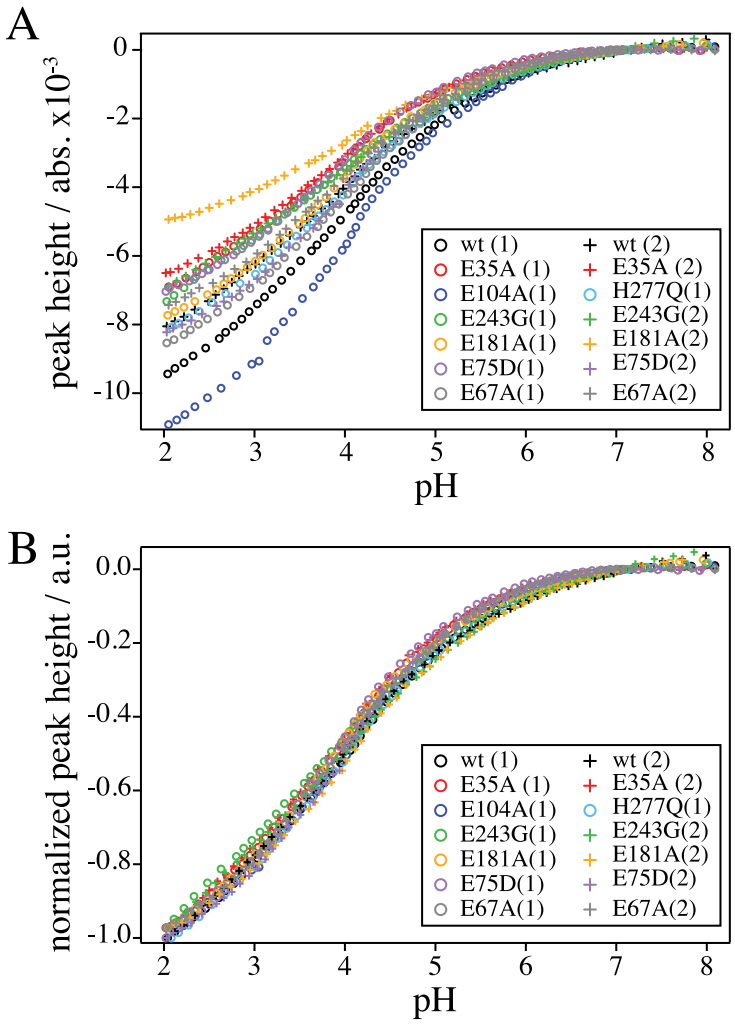

Figure S3. The normalization of nas(COO-) band at 1400 cm-1. (A) Raw and (B) normalized peak heights of the band at 1400 cm-1 on various samples versus pH. The peak height in the latter normalized to zero at pH = 7.0 and -1 at pH 2.0 for WT and H277Q while -0.97 at pH = 2.9 for other mutants. Color codes for WT and mutants are denoted in the inset. (1) and (2) denote data sets that involved different sample preparation.

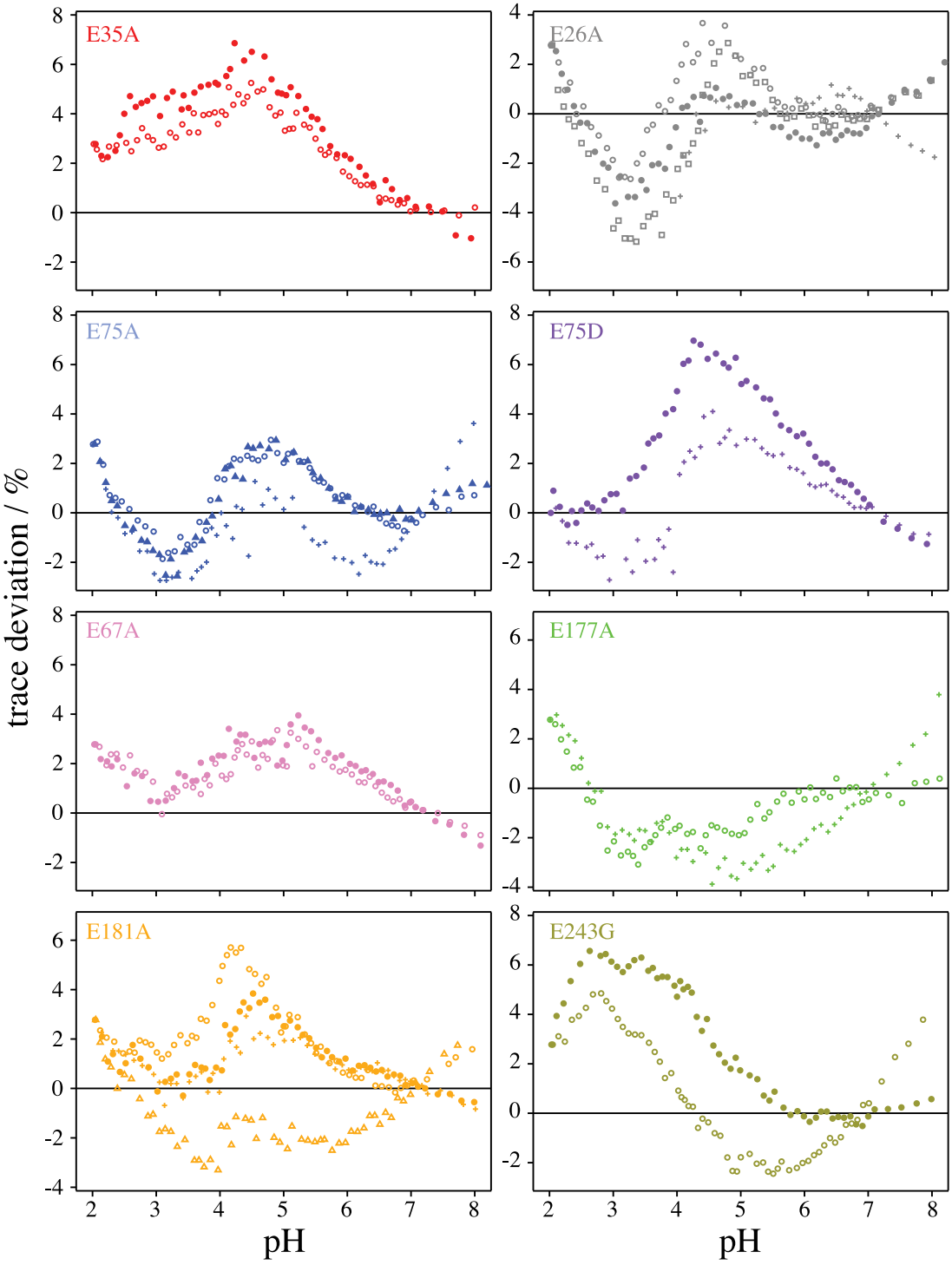

Figure S4. The trace deviation of the pH titration from the wild-type for various mutants. Reproducibility of each mutant had been confirmed by repeating the experiment for two to four times with different sample preparation. Type of mutants are indicated at upper left corner of each figures with different color code. Different markers in each figures represent different set of the measurement. Features of the trace deviation for each mutants are well reproduced, although some data on E75A and E181A show large errors. The latter errors are caused by shift of baseline due to swelling of the lipid depending on pH change. Thus, additional experiments were handled on these mutants to confirm the reproducibility.

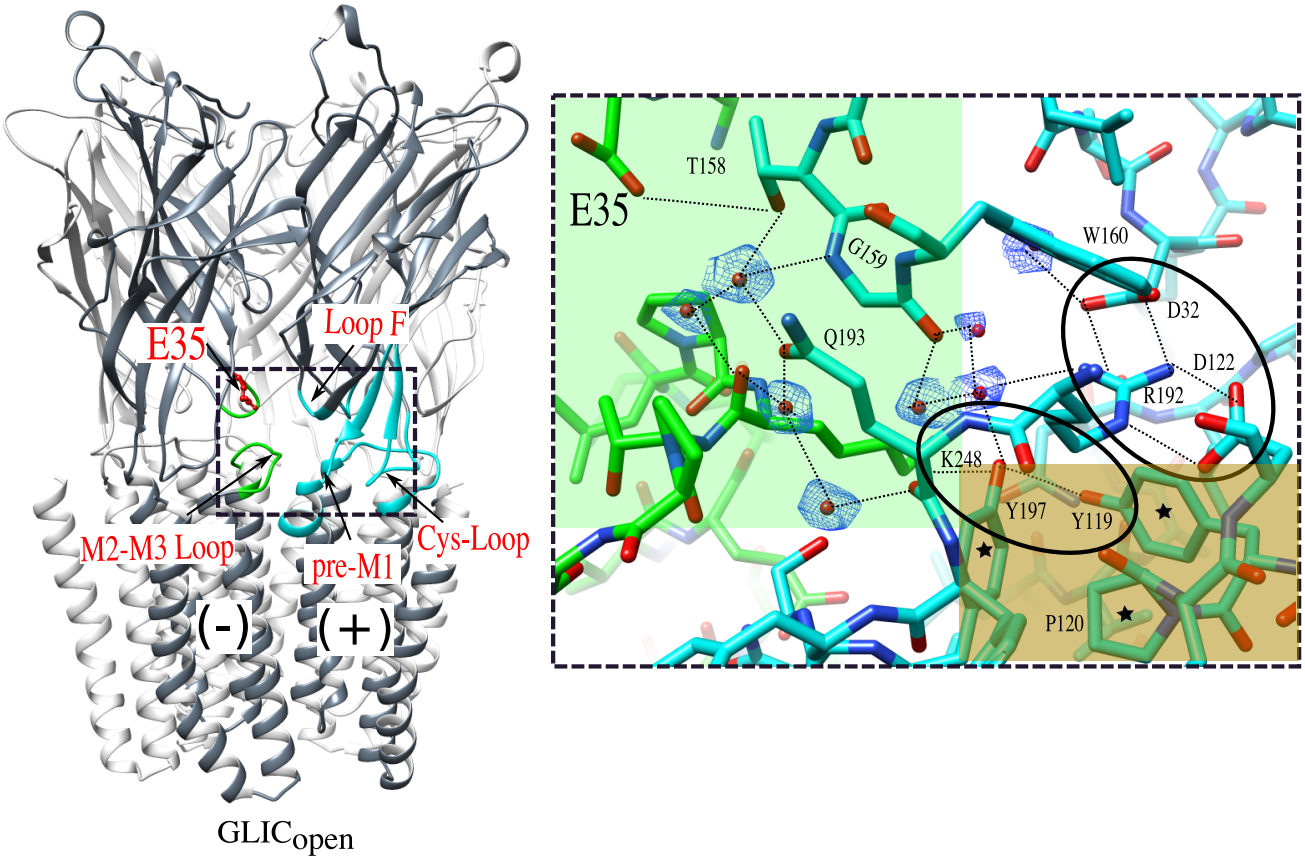

Figure S5. Structurally ordered water molecules at the ECD-TMD interface in the 2.22 Å resolution GLIC open conformation. Water molecules are depicted as red spheres with blue mesh representation of 2mFo-DFc electron density map contoured at a level of 1 σ and overlaid. Surrounding residues are represented as sticks and labeled. Black dashed lines represent the hydrogen bonds network. The "primary" and "secondary" triads are highlighted. Light green region contains ECD-TMD interfacial hydrophilic network; light orange region contains ECD-TMD interfacial hydrophobic network.

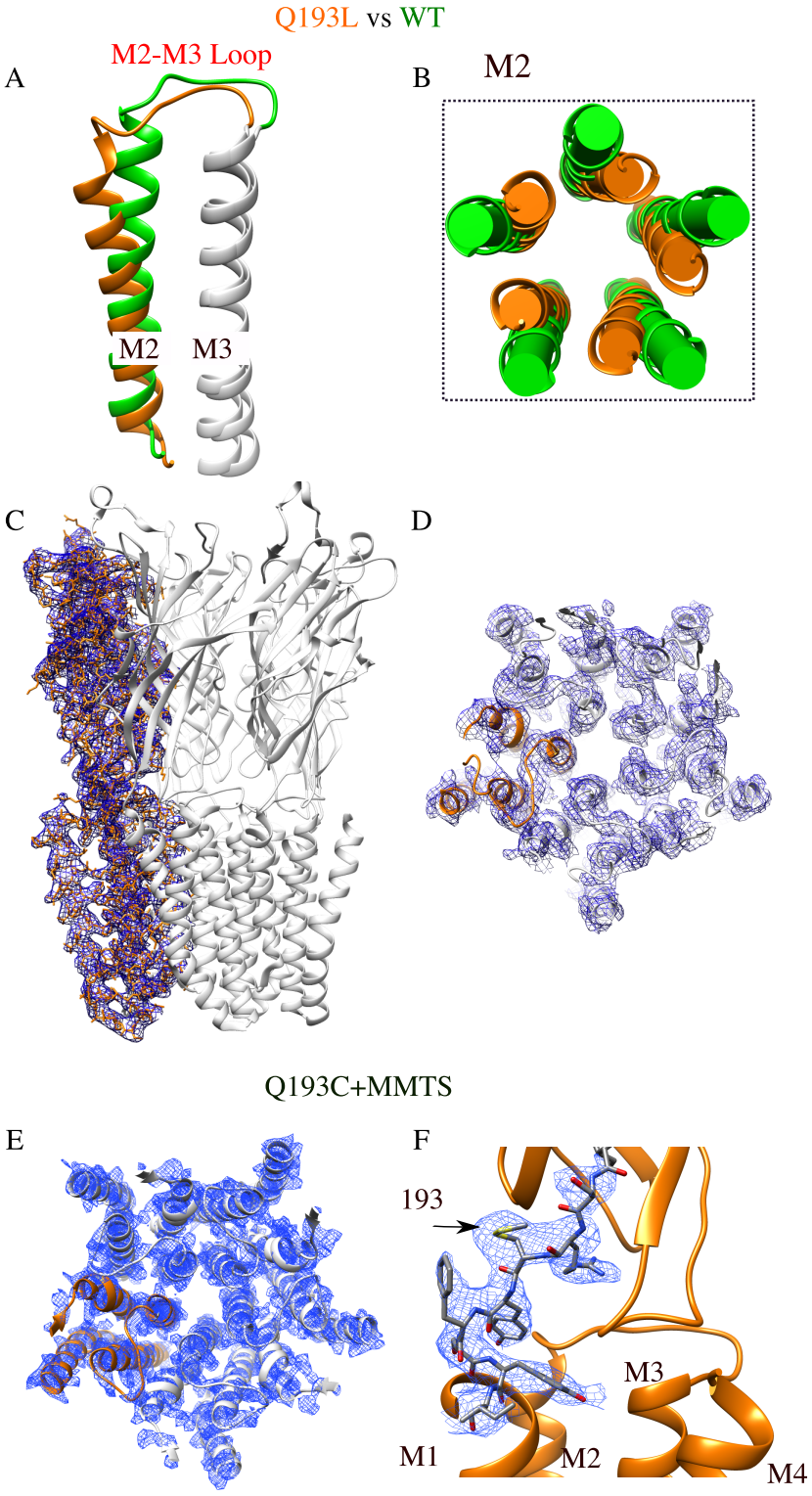

Figure S6. X-ray structure of GLIC Q193L mutant. (A) and (B) show a superimposition of Q193L (orange) with the open form of GLIC (green). (A) M2 helix, M2-M3 loop and M3 helix. (B) Top view of M2 helices conformational change. (C) and (D) show the overall quality of the electron density of the crystal structural of Q193L. (C) 2mFo-DFc electron density (blue) is contoured at the level of 1 σ and is shown superimposed on one of the subunits (orange). (D) Overall quality of the electron density of Q193L TMD, contoured as in C. (E-F) 2mFo – Fc electron density of the Q193C + MMTS complex, contoured at 1 σ.

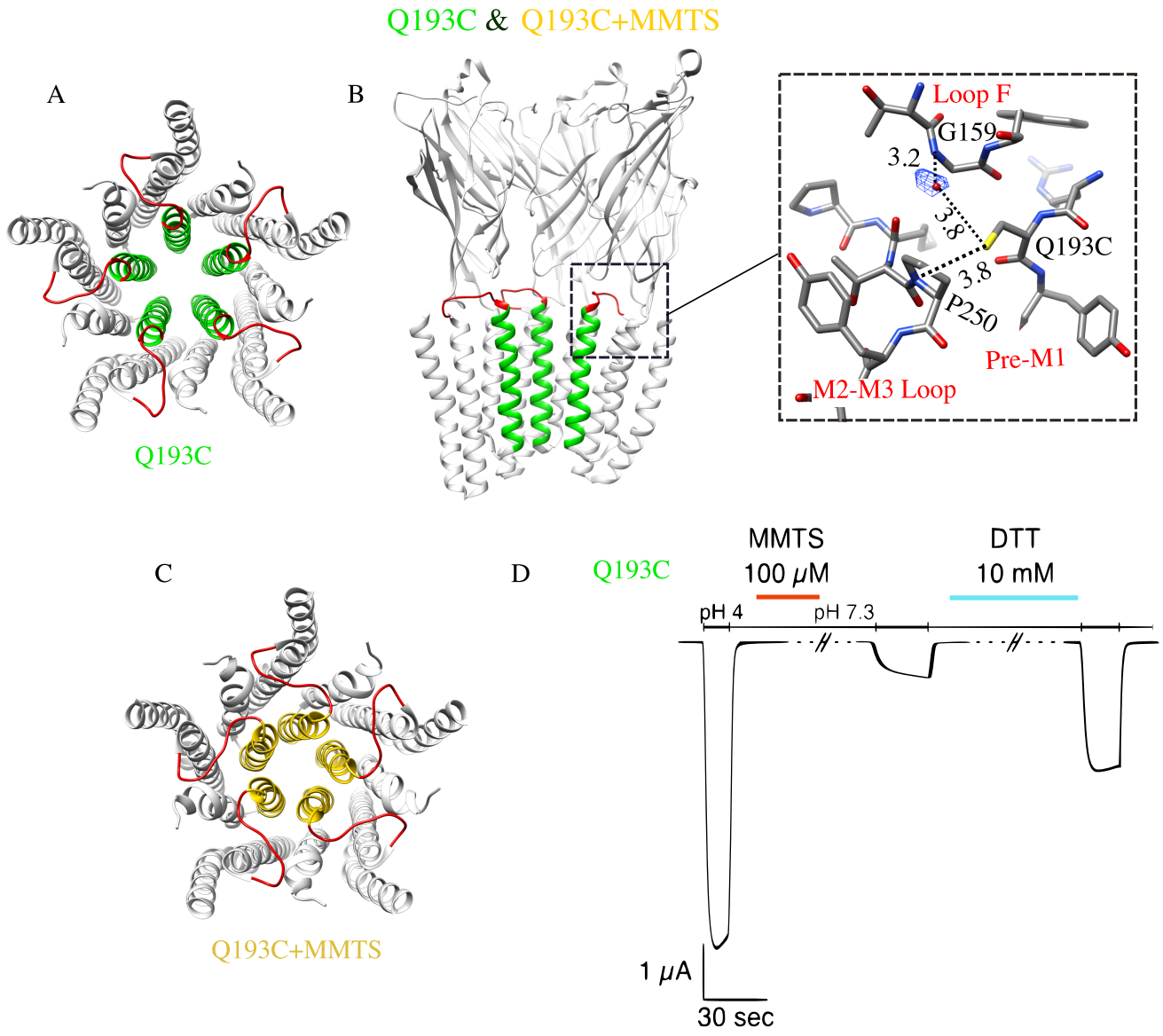

Figure S7. Functional and structural Characterizations of Q193C mutant and chemical labeling. (A) Top view of GLIC Q193C mutant crystal structure with the M2 helices in green and M2-M3 loops red. (B) The left panel shows the side view of GLIC Q193C structure. The right panel shows the electron density map of the interface region corresponding to the rectangle in the left panel. The water molecule is shown as a red sphere and putative hydrogen bonds are shown as dash lines. (C) Crystal structure of Q193C+MMTS. The TMD region is shown with the M2 helices colored as orange and the M2-M3 loop colored as red. (D) Typical electrophysiological recordings of GLIC Q193C. A first pulse at pH 4 is followed by MMTS application at pH 7.3 (4 min) and rinsing (5 min), a second pH 4 pulse is followed by DTT application at pH 7.3 (5 min) and a final pH 4 pulse.

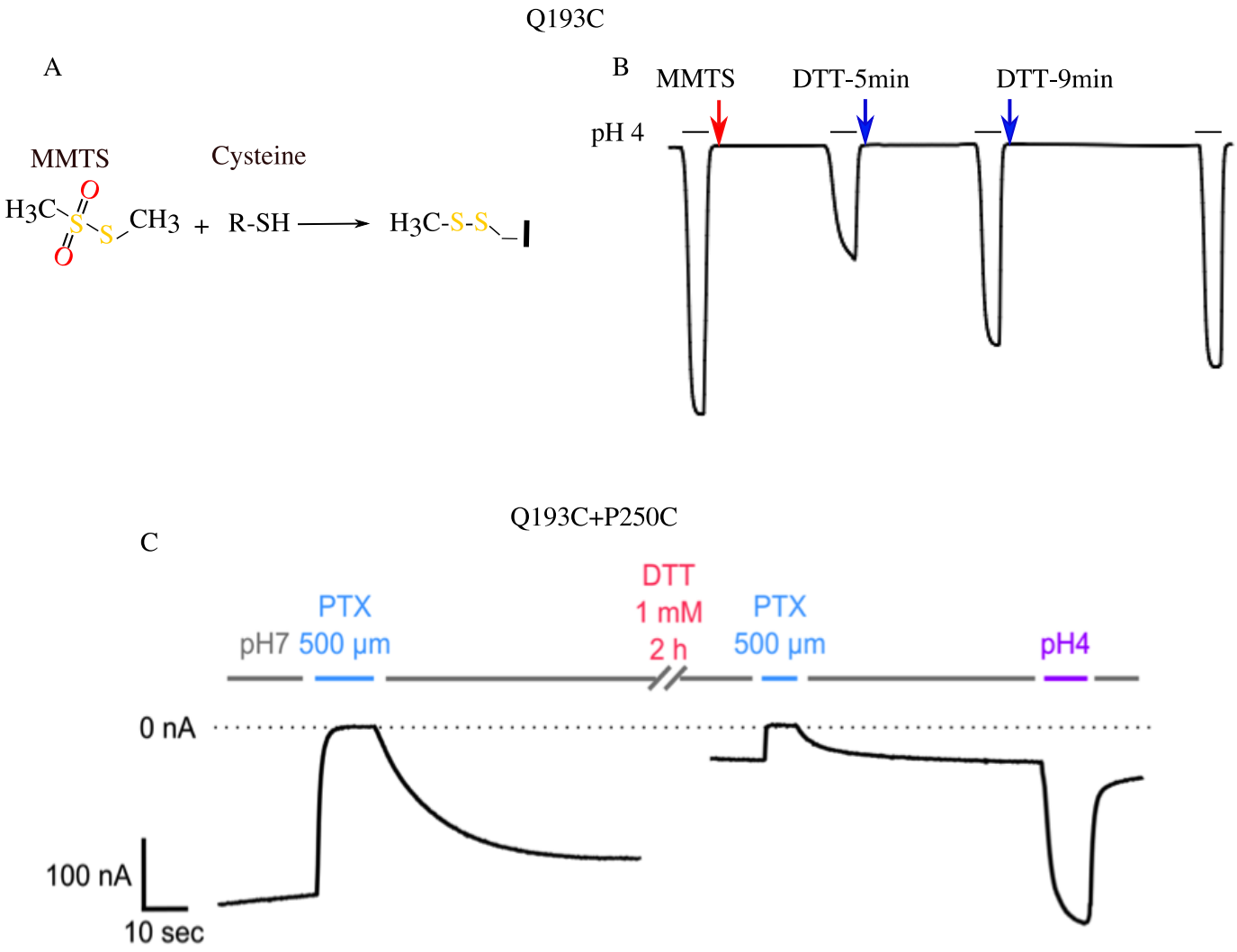

Figure S8. Currents inhibition of Q193C variant by labeling agent MMTS (A-B). (C) Characterisation of the GLIC P250C Q193C mutant. The figure shows a representative electrophysiological recording of GLIC P250C Q193C currents in oocytes clamped at -40 mV. The mutant shows leak current at pH 7 that can be blocked by PTX and abolished by treatment with DTT.

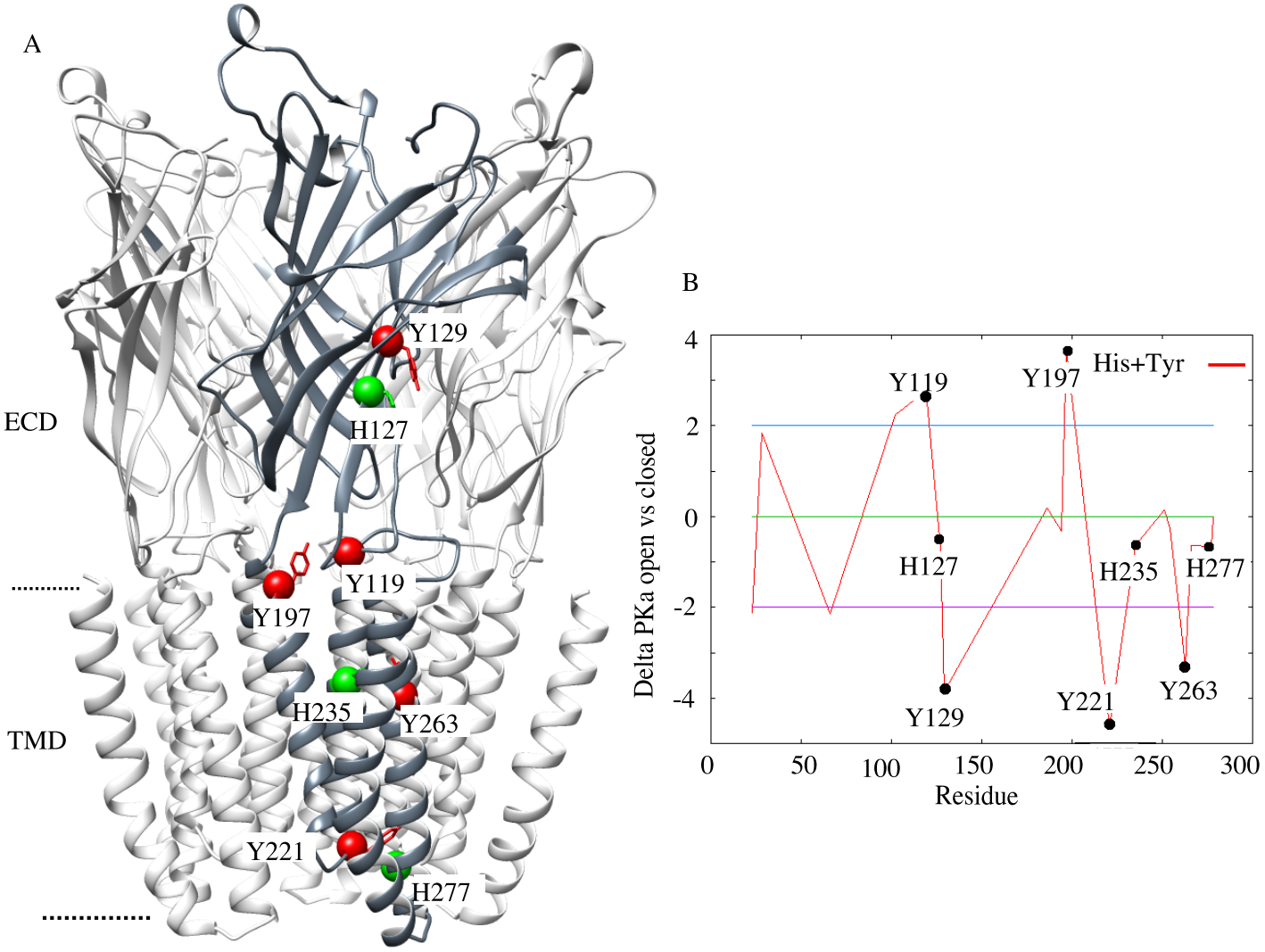

Figure S9. FD-DH predicted pKas for all Tyr residues. (A) Location in the three-dimensional structure of Tyr residues predicted to have strong differences in their pKas in both forms. The two Tyr from the secondary triad are located at the ECD-TMD interface (B) Plots of the ΔpKa as a function of residue number.

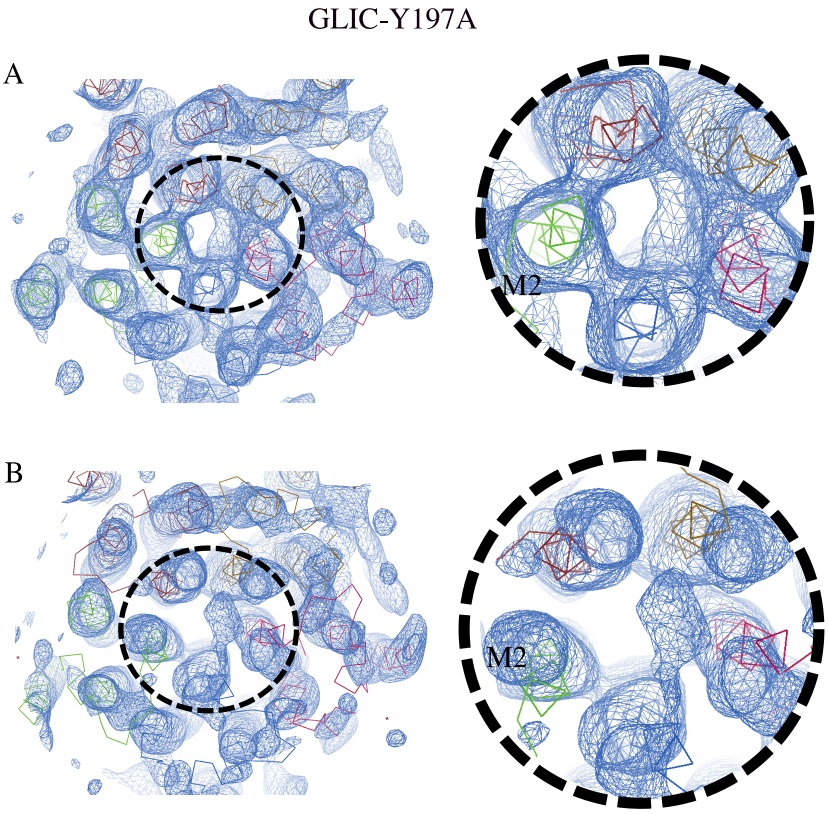

Data collection Channel conformation	GLIC _Y197A Closed
Beamlines	Soleil-PX1 (18/03/2018)
Wavelength (Å)	1.0717
Oscillation range (°)	0.2
Data processing	
Frames	1-1250
Reflections measured	25064(7354)
Reflections unique	5659(1629)
Space group	C 1 2 1
Cell parameters (Å) (°)	175.5 132.4 158.4 90.0 100.37 90.0
Resolution (Å)	29.94-7.00 (7.83-7.00)
Completeness of data (%)	98.5/99.7
Multiplicity	4.4(4.5)
I/sigma (I)	6.5(0.9)
Rmerge	8.6(164.2)
CC ½ (%)	99.9(77.7)

Figure S10. GLIC Y197A adopts LC conformation. (A) 7 Å 2mFo-DFc electron density map (blue) is contoured at the level of 1.3 σ with the dataset refined against the Y197F (LC conformation). (B) 7 Å 2mFo-DFc electron density map (blue) is contoured at the level of 1.3 σ with the same dataset refined against the GLIC WT (Open conformation, PDB ID : 4HFI).

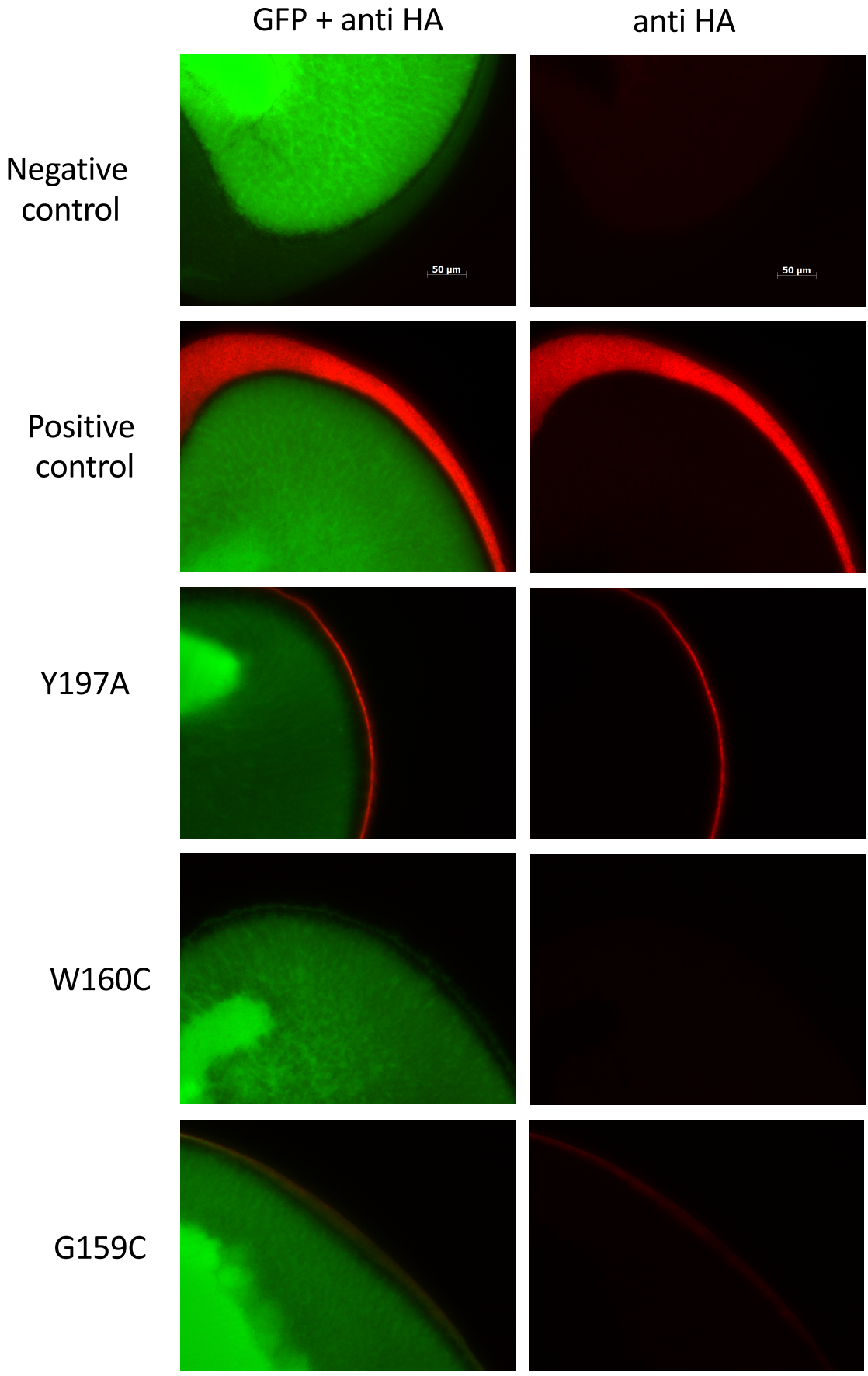

Figure S11: Expression of GLIC nonfunctional mutants (Y197A, W160C, G159C). GFP positive oocytes co-injected with various GLIC-HA mutants, GLIC-HA WT (positive control) or no GLIC (negative control) were labelled with anti-HA fluorophore-conjugated antibodies to assess membrane expression of the different constructs. Immunofluorescence labelling was performed at J+4 post-injection. All images were taken with identical exposure times (10 sec for anti-HA detection).

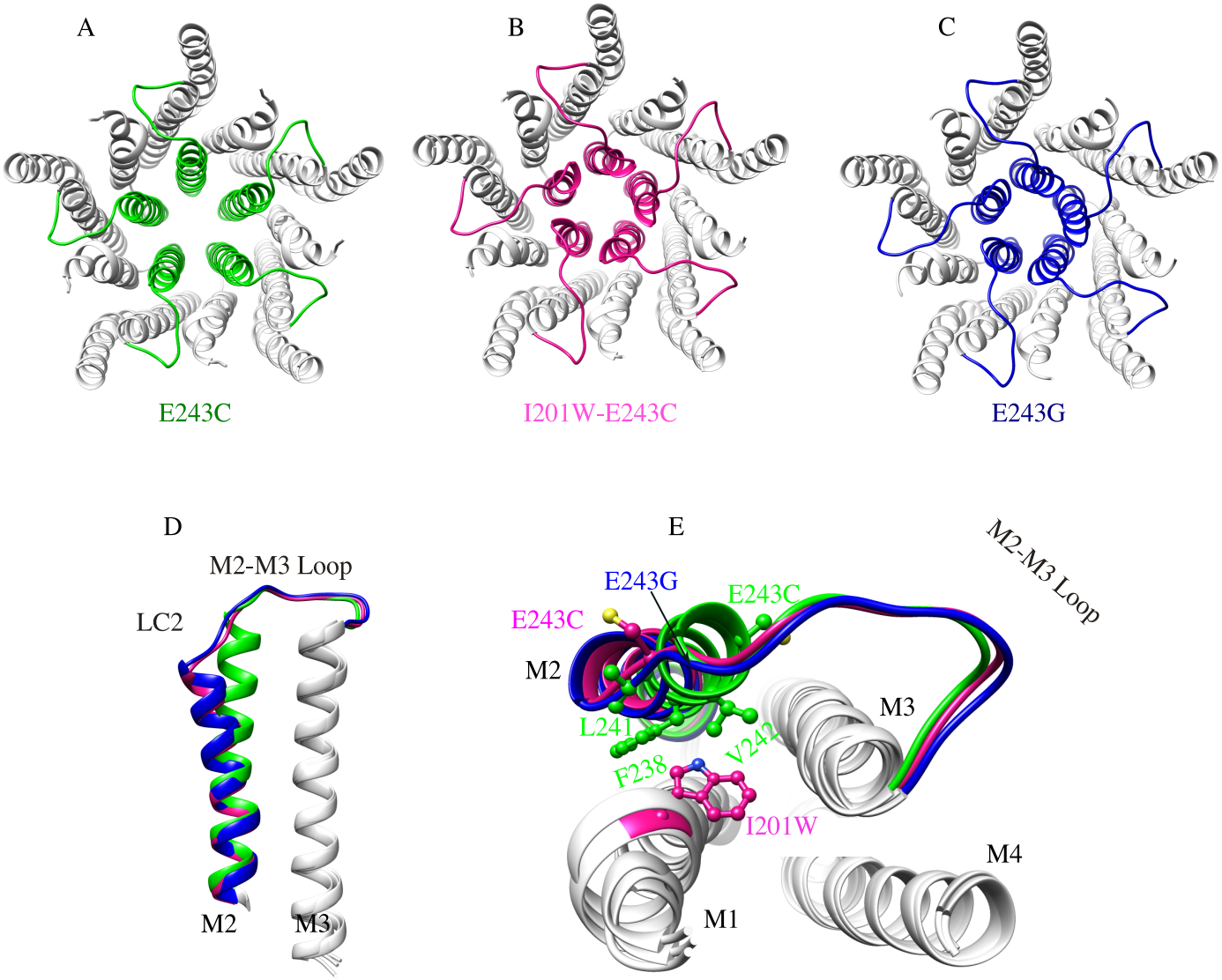

Figure S12. X-ray structures of GLIG mutants at positions E243 and I201. (A)-(C) Ribbon representation TMD of E243C, I210W-E243C and E243G mutant structures. M2 helices and M2-M3 loops are colored in green, magenta, blue, respectively. (D)-(E) Superimposition of the structures of E243C (open form), E243G and I210W-E243C (closed form) showing M2 helix, M2-M3 loop and M3 helix as a side-view (D) or viewed from the top (E). The side chain of W201 is shown as sticks (magenta) in the structure of I201W-E243C and the side chains of F238, L241, V242 are shown as sticks (green) in the structure of E243C.

I201W-E243C

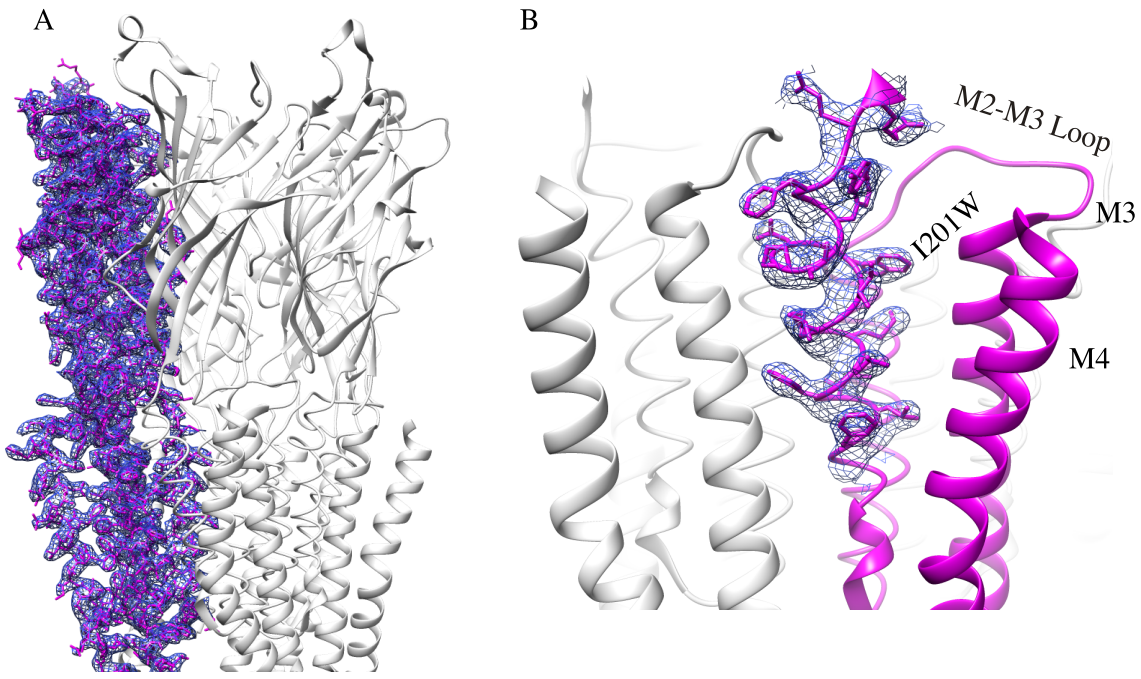

Figure S13. (A) and (B) shows the electron density quality of I201W-E234C. (A) 2mFo-DFc electron density map (blue) is calculated at 2.8 Å and contoured at the level of one σ; it is shown superimposed on one of the subunits (magenta). (B) Electron density quality of the E234C-I201W mutant pre-M1 region. The electron density map is contoured at the level of 1.0 σ and the residue 201W is labeled.

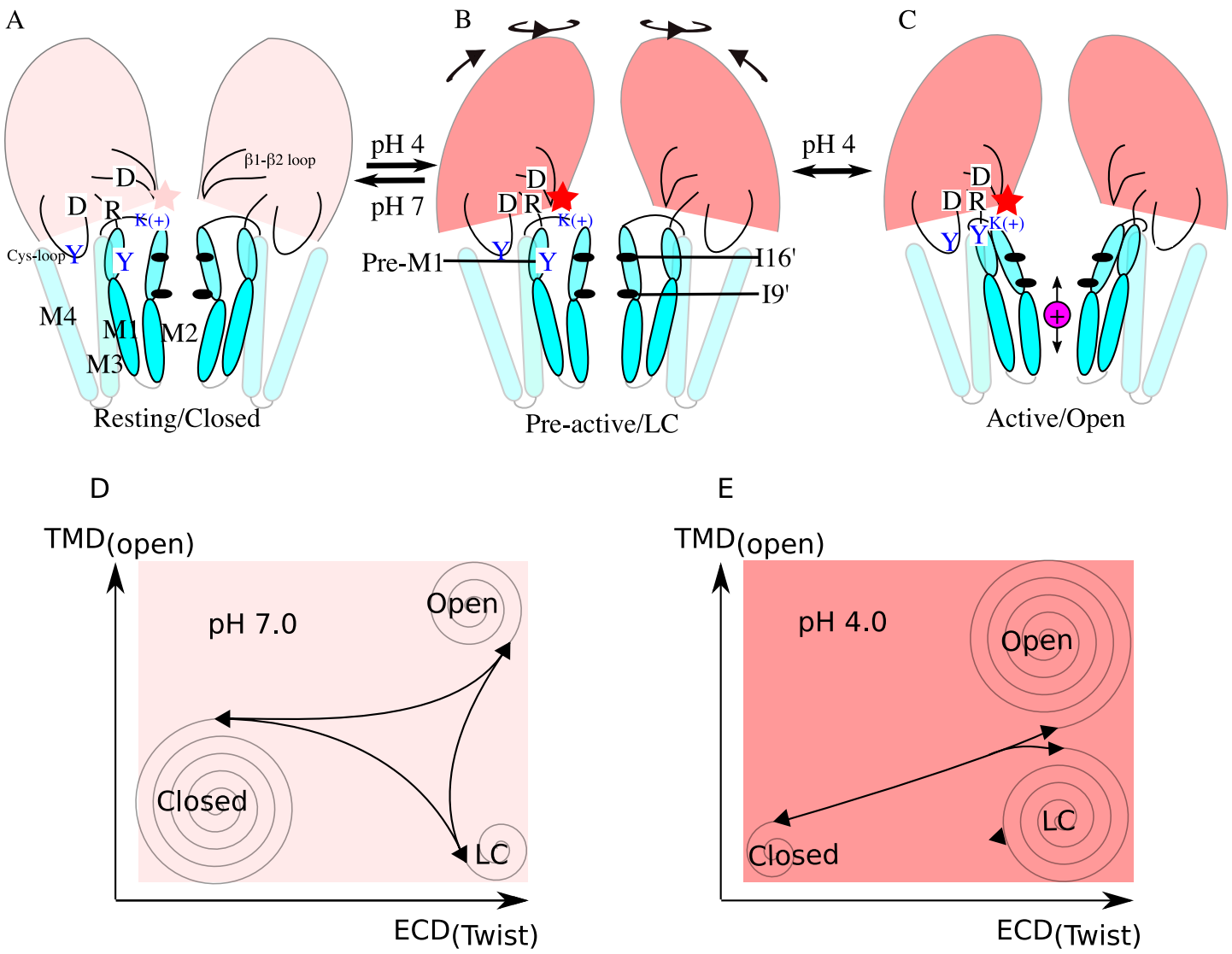

Figure S14. A model for the coupling of proton(s)-binding to channel gating during activation of GLIC. (A-C) Possible model for GLIC activation. The key proton-sensor residue (E35) is indicated in deep red star in LC form (B) and open form (C). Residues involeved in the two electrostatic triads are shown. K(+) represents residue from adjacent subunit. (D-E) Energy landscape inferred from crystal structures of resting GLIC, LC-form, and GLIC Open. (D): pH 7.0; (E): pH 4.0.

Supplementary Table 1: Summaries of electrophysiological experiments.

Mutant	pH_{50}	ΔpH_{50}	Phenotype	Note
WT	5.2 ± 0.4			Nemecz, Á. *et al.* (Ref. 40)
E26A	4.3 ± 0.2	-1.2 ± 0.3	Loss of Function	Nemecz, Á. *et al.* (Ref. 40)
E26Q	4.4 ± 0.1	-1.0 ± 0.3	Loss of Function	Nemecz, Á. *et al.* (Ref. 40)
E35A	6.1 ± 0.1	1.0 ± 0.1	Gain of Function	Nemecz, Á. *et al.* (Ref. 40)
E35Q	6.3 ± 0.1	1.3 ± 0.1	Gain of Function	Nemecz, Á. *et al.* (Ref. 40)
E75A	5.6 ± 0.2	0.3 ± 0.5	Wild-type	Nemecz, Á. *et al.* (Ref. 40)
E104A	4.8 ± 0.2	-0.6 ± 0.2	Wild-type	Nemecz, Á. *et al.* (Ref. 40)
E181A	5.6 ± 0.1	NA	Wild-type	Prevost, M. A. *et al* (Ref. 42)
E181Q	4.9 ± 0.3	-0.5 ± 0.5	Wild-type	Nemecz, Á. *et al.* (Ref. 40)
D32N	4.0 ± 0.2	-1.1 ± 0.2	Loss of Function	Nemecz, Á. *et al.* (Ref. 40)
D32A	NF	NF	Nonfunctional	Bertozzi, C. *et al.* (Ref 18)
D122N	NF	NF	No Expression	Nemecz, Á. *et al.* (Ref. 40)
D122A	NA	NA	Loss of Function	Bertozzi, C. *et al.* (Ref 18)
E67A	5.1 ± 0.1	0.0 ± 0.2	Wild-type	Nemecz, Á. *et al.* (Ref. 40)
E82A	5.0 ± 0.3	-0.5 ± 0.2	Wild-type	Nemecz, Á. *et al.* (Ref. 40)
D86N	4.6 ± 0.1	-0.4 ± 0.1	Wild-type	Nemecz, Á. *et al.* (Ref. 40)
D86A	4.7 ± 0.1	-0.3 ± 0.1	Wild-type	Nemecz, Á. *et al.* (Ref. 40)
D88N	5.0 ± 0.2	-0.4 ± 0.1	Wild-type	Nemecz, Á. *et al.* (Ref. 40)
D88A	4.7 ± 0.2	-0.7 ± 0.2	Wild-type	Nemecz, Á. *et al.* (Ref. 40)
D97N	5.7 ± 0.2	-0.4 ± 0.7	Wild-type	Nemecz, Á. *et al.* (Ref. 40)
H127N	5.7 ± 0.1	0.1 ± 0.1	Wild-type	Nemecz, Á. *et al.* (Ref. 40)
H127Q	4.9 ± 0.3	-0.5 ± 0.5	Wild-type	Nemecz, Á. *et al.* (Ref. 40)
H235Q	4.1 ± 0.2	-1.4 ± 0.2	Loss of Function	Nemecz, Á. *et al.* (Ref. 40)
H277Q	4.6 ± 0.3	-0.6 ± 0.5	Wild-type	Nemecz, Á. *et al.* (Ref. 40)

NA represents that data is not available. NF means nonfunctional receptor. Significance of the results was determined as values larger than 0.5 pH units for the mean ΔpH_{50}, ***and*** mean pH_{50}, as compared to Wt (See Ref. 40).

Supplementary Table 2
Electrophysiology: Functional characteristics of mutants shown in this study.

Mutant	pH_{50}	EC_{50} (μM)	nH	Imax (μA)	n
Wild-type	5.1 ± 0.2	8 ± 3	1.8 ± 0.4	5 ± 1	3
C27S T158C	5.3 ± 0.3	6 ± 3	2.5 ± 0.4	7.2 ± 1.8	4
C27S G159C	NF	NF	NF	NF (> 500 nA)	3
C27S W160C	NF	NF	NF	NF (> 50 nA)	3
C27S Q193C	5.0 ± 0.1	10 ± 3	1.8 ± 0.4	5 ± 2	5
Q193L	4.47 ± 0.06	34 ± 4	2.3 ± 0.2	1.1 ± 0.4	4
Q193M	4.5 ± 0.1	29 ± 8	2.1 ± 0.3	1.0 ± 0.3	5
Y197A	NF	NF	NF	NF (> 100 nA)	4
C27S P250C Y197F	5.2 ± 0.1	6 ± 2	1.3 ± 0.3	4.1 ± 0.1	5

pH_{50}, EC_{50} and nH values were obtained through individual fits of dose-response current curves to the Hill equation. NF stands for non-functional and was used for mutants with currents smaller than 500 nA. n represents the number of experiments. For all the data, mean values and the corresponding standard deviations are presented.

Supplementary Table 3: Diffraction data collection and model refinement statistics.

Data collection Channel conformation PDB ID	GLIC _wt Open PDB ID 6HZW	GLIC _Q193C Open PDB ID 6HY5	GLIC_Q193C+MTS Closed PDB ID 6HYR	GLIC_Q193M Closed PDB ID 6HY9	GLIC_Q193L Closed PDB ID 6HYA	GLIC_Y197F-P250C Closed PDB ID 6HYX
Beamlines	Soleil-PX1 (11/10/2015)	Soleil-PX1 (11/10/2015)	ESRF ID30A (16/11/2015)	ESRF ID29 (04/10/2015)	Soleil-PX1 (11/10/2105)	Soleil-PX1 (11/10/2015)
Wavelength (Å)	0.9771	0.9785	0.9660	0.9789	0.9789	0.9785
Oscillation range (°)	0.05	0.20	0.25	0.10	0.20	0.2
Data processing						
Frames	1-2300	1-1100	1-625	1-1998	1-1100	1-900
Reflections measured	403054(20400)	483142(118354)	122901(12973)	306114(17108)	164069 (13857)	262812(15664)
Reflections unique	169456(8611)	24539(5864)	39511(4461)	76643(4435)	50723(4351)	75432(4436)
Space group	C 1 2 1	C 1 2 1	C 1 2 1	C 1 2 1	C 1 2 1	C 1 2 1
Cell parameters (Å) (°)	182.4 133.4 160.4 90.0 102.5 90.0	182.4 133.5 161.0 90.0 102.2 90.0	179.0 128.3 160.4 90.0 101.0 90.0	182.0 134.4 159.2 90.0 101.5 90.0	181.2 133.3 157.7 90.0 100.9 90.0	182.8 133.2 160.3 90.0 102.1 90.0
Resolution (Å)	49.39-2.22 (2.26-2.22)	49.64-2.58 (2.62-2.58)	49.73-3.50 (3.85-3.50)	49.40-2.95 (3.01-2.95)	48.84-3.39 (3.50-3.39)	49.37-3.00 (3.06-3.00)
Completeness of data (%)	91.9/94.5	99.9/100.0	99.3/99.7	97.0/95.6	99.1/92.6	99.5/99.0
Multiplicity	2.4(2.4)	4.1(4.2)	3.1(2.9)	4.0(3.9)	3.2(3.2)	3.5(3.5)
I/sigma (I)	8.7(1.0)	7.9(1.1)	6.4(1.2)	7.0(1.2)	4.9(1.4)	12.9(9)
Rmerge	4.9(84.1)	9.8(111.9)	10.7(107.6)	8.8(107.5)	6.5(40.6)	4.8(162.4)
CC ½ (%)	99.7(67.8)	99.9(31.7)	99.8(62.3)	99.8(58.1)	99.9(78.2)	99.9(73.2)
Refinement						
Resolution (Å)	20.00-2.22	20.00-2.58	20.00-3.50	20.00-2.95	20.00-3.39	20.00-3.00
Rfactor (%)	19.6	19.9	23.1	20.3	18.5	19.9
Rfree (%)	22.0	20.5	24.1	22.7	21.2	21.3
No. of protein atoms	12715	12610	12620	12620	12620	12620
No. of water molecules	564	274	-	250	-	-
B factor overall ($Å^2$)	37.84	53.57	100.19	84.19	110.86	73.64
B factor for protein ($Å^2$)	36.77	53.10	100.22	84.25	110.94	73.71
B factor for ligands ($Å^2$)	62.52	78.90	82.38	37.15	59.09	35.71
B factor for solvent ($Å^2$)	41.00	41.00	-	78.00	-	-
Ramachandran outliers (%)	0	0	0	0	0	0
RMSD bond lengths (Å)	0.010	0.010	0.008	0.010	0.010	0.010
RMSD bond angles (°)	1.06	1.06	0.98	1.10	1.12	1.08

Data collection Channel conformation PDB ID	GLIC_Y119A Open 6HYV	GLIC_Y119F Open 6HYW	GLIC_K248C Open 6HYZ	GLIC_K248A Open 6HZ0	GLIC_E243C Open 6HZ1	GLIC_E243G Closed 6HZ3	GLIC_E243C_I20W Closed 6I08
Beamlines	Soleil-PX2 (18/12/2016)	ESRF ID30A (28/10/2016)	ESRF ID_30b (27/07/2015)	ESRF ID_30b (27/07/2015)	ESRF ID23 (04/05/2016)	ESRF ID_30B (27/07/2015)	ESRF ID30A (25/11/2016)
Wavelength (Å)	0.9785	0.9771	0.9801	0.9801	0.984	0.9762	0.9677
Oscillation range (°)	0.20	0.05	0.10	0.10	0.10	0.05	0.10
Data processing							
Frames	1-900	1-2300	1-5500	1-3600	1-1090	1-4500	1-3000
Reflections measured	317806(15428)	199056(9491)	290473 (19361)	503908 (23214)	265150 (12934)	230620 (17589)	333573 (21292)
Reflections unique	90262(4387)	85783(4345)	70102(4547)	94881(4690)	122120(6048)	61001(4519)	73894(4607)
Space group	C 1 2 1	C 1 2 1	C 1 2 1	C 1 2 1	C 1 2 1	C 1 2 1	C 1 2 1
Cell parameters (Å) (°)	180.8 132.4 159.7 90.0 102.2 90.0	183.0 132.2 161.5 90.0 103.2 90.0	181.2 132.9 160.0 90.0 102.0 90.0	180.9 132.7 159.3 90.0 102.0 90.0	180.9 133.0 160.1 90.0 102.4 90.0	177.5 129.1 159.6 90.0 101.0 90.0	180.8 134.3 159.4 90.0 101.8 90.0
Resolution (Å)	49.23-2.80 (2.85-2.80)	48.34-2.80 (2.85-2.80)	49.32-3.05 (3.12-3.05)	49.14-2.75 (2.80-2.75)	49.07-2.50 (2.54-2.50)	49.12-3.15 (3.23-3.15)	48.90-3.00 (3.06-3.00)
Completeness of data (%)	99.8/99.8	93.2/89.7	99.1(99.9)	99.3(98.8)	95.6(95.7)	99.7(99.9)	99.0/99.8
Multiplicity	3.5(3.5)	2.3(2.2)	4.1(4.3)	5.3(4.9)	2.1(2.1)	3.8(3.9)	4.5(4.6)
I/sigma (I)	9.7(1.2)	9.9(1.2)	7.7(1.1)	9.6(1.0)	8.2(1.5)	5.6(1.0)	12.5(1.6)
Rmerge	7.7(96.0)	5.7(39.6)	6.2(79.2)	5.0(85.4)	5.7(46.1)	10.8(108.8)	4.0(58)
CC ½ (%)	99.8(65.9)	99.8(79.7)	99.9(86.2)	100.0(88.2)	99.9(65.6)	99.8(78.0)	100.0(94.6)
Refinement							
Resolution (Å)	20.00-2.80	20.00-2.80	20.00-3.05	20.00-2.75	20.00-2.50	20.00-3.15	20.00-2.80
Rfactor (%)	20.9	19.3	22.6	21.0	19.8	23.0	22.2
Rfree (%)	22.1	21.2	23.4	23.8	21.1	24.9	23.7
No. of protein atoms	12615	12660	12610	12695	12661	12600	12640
No. of water molecules	117	236	95	320	230	32	260
B factor overall (Å^2)	45.01	47.02	102.74	71.30	49.30	41.97	44.63
B factor for protein (Å^2)	44.41	46.49	101.81	70.87	48.83	42.03	44.61
B factor for ligands (Å^2)	59.33	64.40	132.13	91.02	67.90	31.22	74.99
B factor for solvent (Å^2)	37.17	44.93	79.39	58.86	36.68	18.79	60.00
Ramachandran outliers (%)	0	0	0	0	0	0	0
RMSD bond lengths (Å)	0.010	0.010	0.009	0.010	0.009	0.009	0.010
RMSD bond angles (°)	1.13	1.06	1.13	1.02	1.03	1.07	1.11

Supplementary Notes

August 2, 2018

1 Introduction

In these notes we recall some basic results about a pH-driven transition when there are two conformational states of the molecule (open vs closed). We then describe the consequences of this formalism to analyze the difference traces of various GLIC mutants obtained by the FT-IR method.

2 Simple model for a proton-driven transition (single site)

Let us describe first a simple chemical model with a single titrable charged residue (Asp or Glu) for a molecule that can exist in two forms (open and closed), protonated or not.

$$\begin{array}{ccc} & \overset{K_D \text{ at } pH\ 7}{} & \\ H^+ + Closed^- & \rightleftharpoons & H^+ + Open^- \\ \updownarrow & & \updownarrow \\ Closed - H & \rightleftharpoons & Open - H \\ & \underset{K_H \text{ at } pH\ 4}{} & \end{array} \tag{1}$$

We take the following definition for the equilibrium constants:

$$K_D = \frac{(Closed^-)}{(Open^-)} \quad K_H = \frac{(Closed - H)}{(Open - H)} \tag{2}$$

with $\Delta G_D = -RT \log K_D$ and $\Delta G_H = -RT \log K_H$. Because of the thermodynamic cycle we have

$$K_D = K_H \frac{K_a^{Closed}}{K_a^{Open}} \tag{3}$$

which can be translated into the linear relationship $\Delta\Delta G = \Delta G_D - \Delta G_H = 2.303\ RT \Delta pK_a$.

As the channel must be mainly closed at pH 7 and open at pH 4, we assume $K_H << 1$ and $K_D >> 1$.

If we can calculate the quantities $pK_a^{(o)}$ and $pK_a^{(c)}$, for instance by the FD-DH Method described by Sazanavets and Warwicker (2015), then we are left with only one unknown, K_D (or K_H).
We reproduce below these calculations for all residues having a carboxylate group (Asp and Glu).

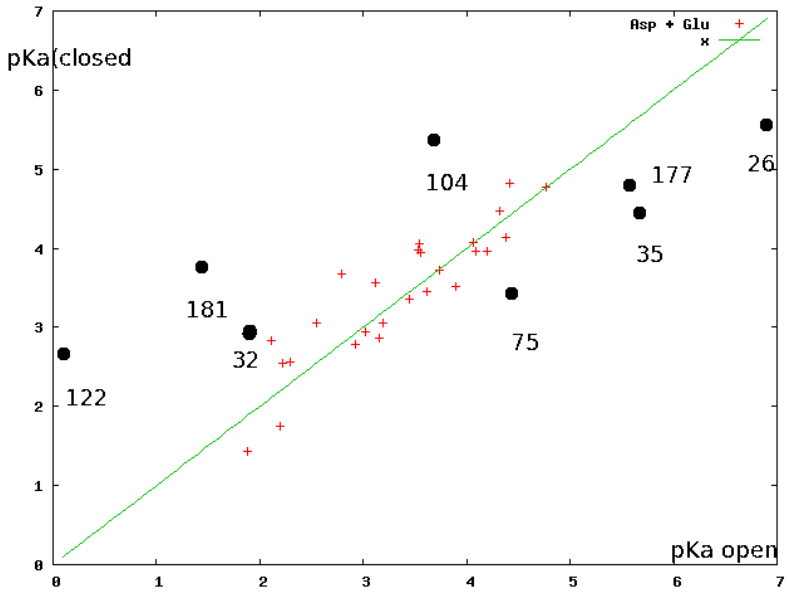

Suppl. Notes Fig. N1. Calculated pK_a for the closed form vs predicted pK_a in the open form

3 FT-IR titration experiments

We wish to understand/explain the shape of the pH-induced transitions monitored by FT-IR. First we treat the case of a single titrable residue at position i.

Following Roitberg et al., 2012, we write the signal S_i observed as a function of α_i and β_i that represent the absorption coefficients of the two species charged and uncharged, respectively.

$$S_i = \alpha_i((C-) + (Op-)) + \beta_i((CH) + (OpH)) \tag{4}$$

We have found it useful to rewrite the formula in the following way, having set $\Delta pK_a = pK_a^{(c)} - pK_a^{(o)}$

$$S_i = \alpha_i + (\beta_i - \alpha_i)\frac{1}{1 + \frac{1+K_D}{1+K_D e^{-2.303\Delta pKa}} e^{2.303(pH - pK_a^{(c)})}} \tag{5}$$

This (new) formula has the following required properties that its values are α_i and β_i at the extremes points of the pH titration. Obviously, we need $\alpha_i \neq \beta_i$ to observe a signal.
We note that Eq. 6 is the same as the one given in Liu et al. (2018), after some rearrangements.

There are three main cases, depending on the sign of $(\Delta pK_a - \log_{10} K_D)$ and assuming $K_D >> 1$
1. If $1 + K_D e^{-2.303\Delta pKa} \approx 1$ (i.e. $\Delta pK_a > 1 + \log K_D \approx 2$)

$$S_i \approx \alpha_i + (\beta_i - \alpha_i)\frac{1}{1 + K_D e^{2.303(pH - pK_a^{(c)})}} \tag{6}$$

and we see that $pK_a^{app} = pK_a^{(c)} + \Delta G_D / 2.303RT$:
Compared to $pK_a^{(c)}$ the apparent pK_a^{app} is shifted by a value that depends on K_D.

This would typically be the case of E104A or E181A (D32 and D122 could not be tested).
2. If $1 + K_D e^{-2.303\Delta pKa} \approx K_D e^{-2.303\Delta pKa}$ or $\Delta pK_a < 0$

$$S_i \approx \alpha_i + (\beta_i - \alpha_i)\frac{1}{1 + e^{2.303(pH - pK_a^{(o)})}} \tag{7}$$

and we see that $pK_a^{app} \approx pK_a^{(o)}$ with no dependency on K_D.
This would typically be the case of E35A mutant ($pK_a^{(c)} = pK_a^{(o)} + 1.2$) or E75A (or E177A or E26A).
3. If $\Delta pK_a \approx 0$ and taking into account $K_D >> 1$

$$S_i \approx \alpha_i + (\beta_i - \alpha_i)\frac{1}{1 + e^{2.303(pH - pK_a^{(c)})}} \tag{8}$$

and we see that $pK_a^{app} \approx pK_a^{(c)}$ with no dependency on K_D.
This would typically be the case of E243G mutant ($pK_a^{(c)} = pK_a^{(o)}$).

We have written a small Fortran code to simulate transition curves.
It would also be possible to calculate explicitly pK_a^{app} as a function of K_D and ΔpK_a by writing Eq. (6) as:

$$S_i \approx \alpha_i + (\beta_i - \alpha_i)\frac{1}{1 + e^{2.303(pH - pK_a^{app})}} \tag{9}$$

The point here is that $pK_a^{app} = pH_{50}$ depends on $K_D, pK_a^{(o)}, pK_a^{(c)}$ (see also Roitberg and coll., 2012; 2018) and that we need to know at least the sign of $\log K_D - \Delta pK_a$ to know what we are actually measuring with pH_{50}, even for a protein with a *single* titrating group.

4 Mutants and Difference Titration curves

If there are N titrable groups, and if they are assumed to be independent, one can write the signal of the wild-type:

$$S_{wild-type} = \sum_{i=1,N} S_i \tag{10}$$

For any mutant we can calculate the difference curve $\Delta S = S_{wild-type} - S_{mutant}$.
Denoting by j the site of the mutation, we have

$$\Delta S^{(j)} = \sum_{i=1,N} S_i^{wt} - \sum_{i \neq j} S_i^{mut} = S_j - \sum_{i \neq j} \delta S_i^{(j)} \tag{11}$$

where $\delta S_i^{(j)}$ represents the change in S_i caused by the mutation at site j through a change in either K_D or pK_a.
In a first approximation, one can say that $\Delta S^{(j)} \approx S_j$, i.e. the difference of the titration traces mutant vs wild-type gives the titration curve of the mutated residue.

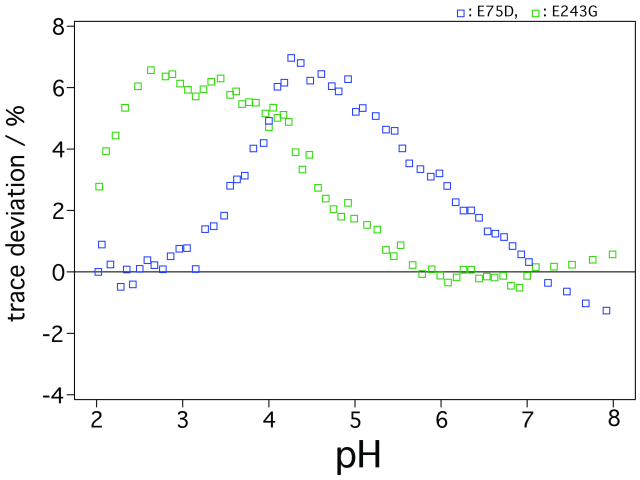

Suppl. Notes Fig. N2. Difference (in %) of FT-IR titration curves of E243G (green) and E75D (blue). The wavelength is 1400 cm^{-1} as in Fig. 2 of the main text.

5 E75D and E243G mutants

Here we present two mutants of interest that "validate" our previous approach.
E243G present a typical titration curve, shown in Fig. 3 in green, with $pH_{50} = 4.5$, which indicates that the region of the titration curve $pH = 2.5 - 4$ is useful.

In the mutant E75D, however, we need to apply a specific treatment since the mutation suppresses a carboxylate group and replaces it by another one with a shorter side-chain.
This is done in the following way:
assuming similar α_i and β_i absorption coefficients but different pK_a for the mutants, we can write

$$\Delta S_j = \alpha_1 + (\beta_1 - \alpha_1)F_1(pH, pK_a^{(1)}) - (\alpha_2 + (\beta_2 - \alpha_2)F_2(pH, pK_a^{(2)})) \approx (\beta - \alpha)(F_1(pH) - F_2(pH)) \quad (12)$$

where $F(pH, pK_a) = \frac{1}{1+K_D e^{2.303(pH-pK_a)}}$.

In the Figure 3, we show that we can indeed simulate the titration curves for E243G and E75D.

6 Mutants with $|\Delta pKa| > 1$

In Figure 4 we show the experimental data for the mutants with $|\Delta pK_a| > 1$, namely 181, 104, 26, 35, 75 and 177.
For E35, the titration curve is well behaved and we can read the pK_a^{app} directly from the data.
For two of the mutants, E75A or E181A, there is a "depression zone" in the range pH-2.5-4.0, but the pKa^{app} can still be estimated.
For the other mutants the signal is completely blurred.
In the following paragraph, we will attempt to explain this behavior.

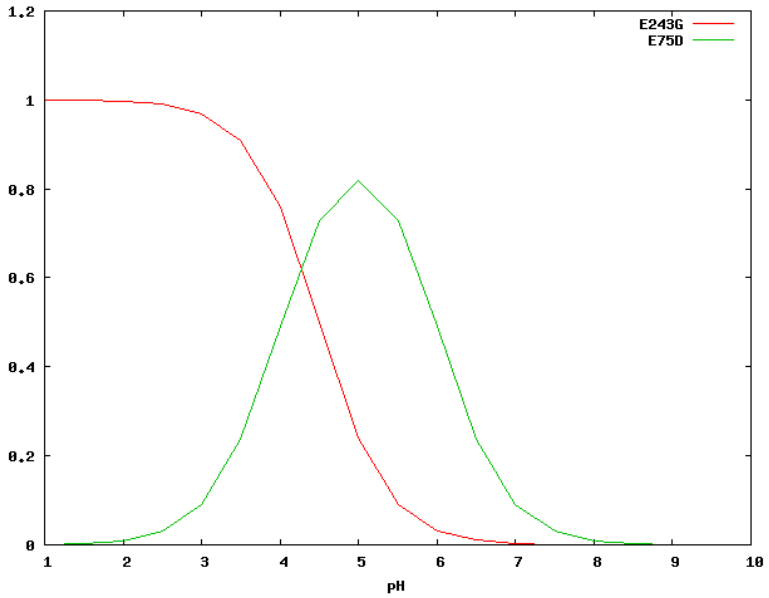

Suppl. Notes Fig. N3. Simulation of the titrations of E243G (red) and E75D (green) using Eq. (x) and (y), respectively.

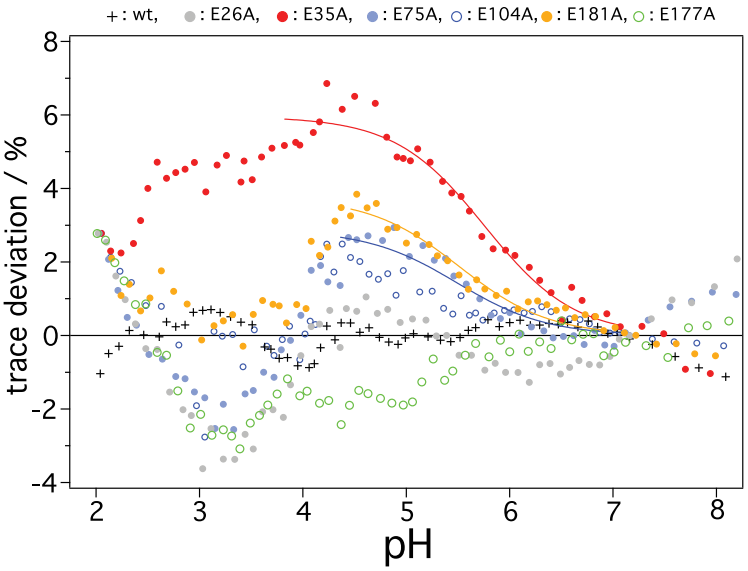

Suppl. Notes Fig. N4. Difference (in %) of FT-IR titration curves for GLIC Mutants with $|\Delta pK_a| > 1$. The wavelength is 1400 cm^{-1} as in Fig. 2 of the main text.

7 Correction terms

Here we show how to take into account the corrections (Eq. 12) to the simple-minded view $\Delta S^{(j)} \approx S_j$ by a Taylor expansion to first order.
1. Case 1. For those residues whose signal S_i depends on K_D (Eq. 7):

$$\delta S_i^{(j)} = \frac{\partial S_i^{(j)}}{\partial K_D} \delta K_D \tag{13}$$

We find

$$\frac{\partial S_i^{(j)}}{\partial K_D} = -\frac{(\beta_i - \alpha_i)}{K_D} \frac{1}{1 + K_D e^{2.303(pH - pK_a^{(c))}}} \frac{1}{1 + K_D e^{-2.303(pH - pK_a^{(c)})}} \tag{14}$$

We see that the derivative $\frac{\partial S_i}{\partial K_D}$ is a bell-shaped curve, centered on $pK_a^{(c)}$ (shifted by K_D).
The sum runs on those few residues with $pK_a^{(c)} > pK_a^{(o)}$, such as D122 and E181 that have a low pK_a.
The correction is centered on $pH = 3 - 4$ for residues 181, 122 and 32.
However, this correction is small since there is K_D in the denominator, unless δK_D is large.

2. Case 2. We can estimate the correction for those titrating groups below the diagonal (Eq. 8), which might undergo a δpK_a shift upon the mutation (E35, E75, E177, E26).

$$\delta S_i^{(j)} = \frac{\partial S_i^{(j)}}{\partial pK_a} \delta pK_a \tag{15}$$

This is the same type of bell-shaped curve, but not weighted by $1/K_D$. However, it is not necessarily centered on $pH = 3 - 4$,

$$\frac{\partial S_i^{(j)}}{\partial pK_a^{(o)}} = 2.303(\beta_i - \alpha_i) \frac{1}{1 + e^{2.303(pH - pK_a^{(o)})}} \frac{1}{1 + e^{-2.303(pH - pK_a^{(o)})}} \tag{16}$$

3. Case 3. For those residues where $pK_a^{(o)} \approx pK_a^{(c)}$ the same equation holds, but we have to replace $pK_a^{(o)}$ by $pK_a^{(c)}$. This time, we see that a single change of one pH unit of the pK_a of one titrable group with $pK_a^{(o)} \approx pK_a^{(c)} \approx 3$ is enough to produce a "hole" of about 0.6 pH unit in the zone around pH=3-4.

8 Prediction of pK_a of mutants

Since we have the structure of the open form of some of the mutants described above, we can also run the calculation of FD-DH on them. The result is shown in Figure 5 for those residues that are below the diagonal, in the region of pH_{50}.
We see that E35A is not too much perturbed compared to wild-type GLIC, which is not the case of E75A and E177A or E26A.
For E181A and E104A, we would need the structure of the closed form to calculate the pKas, but it is unfortunately too difficult to get (we could only get the crystal structure of the wild-type at 4.2 Angstrom after screening thousands of crystals), and we cannot compare the pKa predictions of these mutants with ones for the wild-type.

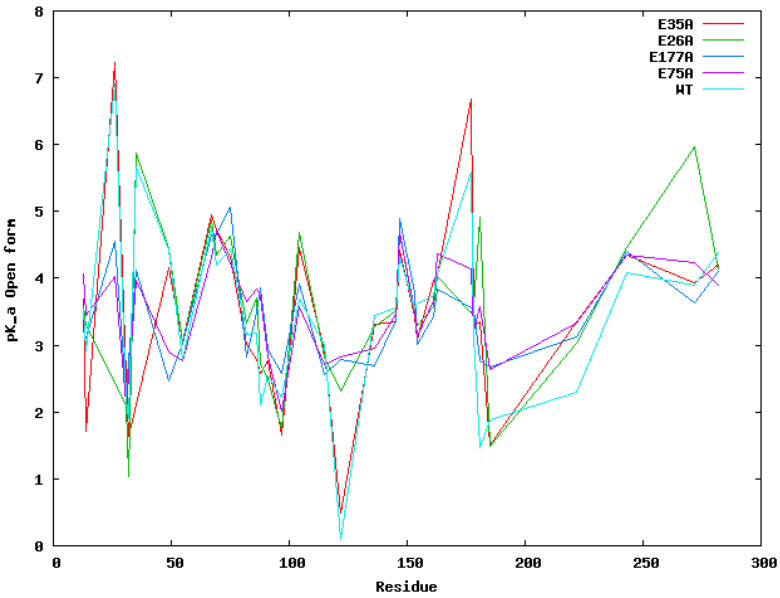

Figure 5: Prediction of pKas for mutants, in the open form, using the FD-DH method.

9 Conclusion

The fact that the mutation might perturb both the K_D and some of the pK_as anywhere in the protein can 'blur' the titration signal by adding an inverted bell-shaped curve to the normal titration curve. Still, the FT-IR method allows to measure individual pK_a if the mutation does not perturb too much the other pK_a (E35A, E243G), which is not the case of electrophysiology methods.
Also, the fact that for E181 the individual pKa is around 5.5 implies that $K_D \approx 20$, which is a measurement that has not been reported before.

10 References

-A. Roitberg and coll. (2012). pH-Dependent conformational changes in proteins and their effect on experimental pK(a)s: the case of Nitrophorin 4. PLoS Comput Biol. 2012 8(11):e1002761.
-I. Sazanavets and J. Warwicker (2015). Computational Tools for Interpreting Ion Channel pH-Dependence. PLoS One 2015 10:e0125923.
-Liu J. et al., (2018). A Coupled Ionization-Conformational Equilibrium Is Required To Understand the Properties of Ionizable Residues in the Hydrophobic Interior of Staphylococcal Nuclease. JACS 2018 140:1639-48.

11 Appendix: Data from the FD-DH program

11.1 Detection of salt bridges using FD/DH

The FD-DH program produces on output a list of interacting titrable residues. We note that it picks up correctly the D122-R192-D32 triad. But it also detects another one Y119-Y197-K248, in the open state.

We reproduce this list here (residue number followed by a + or a - indicate next or previous subunit):

List of coupled pairs with coupling energy (in kT) larger than 4.60 (the ones above 8 kT are underlined)
i-pr = * 1 pair is A 32 ASP and A 192 ARG kT-coupling-energy = 8.75 First Triad
i-pr = * 8 pair is A 122 ASP and A 192 ARG kT-coupling-energy = 8.94 First Triad
i-pr = * 2 pair is A 49 ASP and A 51 ARG kT-coupling-energy = 5.77
i-pr = 3 pair is A 82 GLU and A 109 ARG kT-coupling-energy = 4.66
i-pr = 4 pair is A 85 ARG and A 104 GLU kT-coupling-energy = 5.65 PAM Bzdp Binding site
i-pr = * 6 pair is A 102 TYR and A 104 GLU kT-coupling-energy = 6.92 PAM Bzdp Binding site
i-pr = 5 pair is A 91 ASP and A 179+ ARG kT-coupling-energy = 5.68 Loop C
i-pr = 10 pair is A 133 ARG and A 181 GLU kT-coupling-energy = 5.81 Loop C
i-pr = * 7 pair is A 119 TYR and A 197 TYR kT-coupling-energy = 9.46 2nd Triad
i-pr = *11 pair is A 192 ARG and A 197 TYR kT-coupling-energy = 4.78 1st-2nd Triads link
i-pr = 12 pair is A 197 TYR and A 248+ LYS kT-couplina-energy = 5.81 2nd Triad
i-pr = 15 pair is A 248 LYS and A 119- TYR kT-coupling-energy = 5.62 2nd Triad
i-pr = 16 pair is A 248 LYS and A 197- TYR kT-coupling-energy = 8.92 2nd Triad
i-pr = * 9 pair is A 127 HIS and A 185 ASP kT-coupling-energy = 6.33 His (see also Y129)
i-pr = *13 pair is A 235 HIS and A 263 TYR kT-coupling-energy = 6.16 His
i-pr = *14 pair is A 235 HIS and A 266 TYR kT-coupling-energy = 6.10 His

Interestingly, we see that the R192-D122-D32 triad is connected to the triad Y119-Y197-K248 through the R192-Y197 interaction (#11, underlined).

In the closed state, the pairs noted with * are conserved, the other are lost.
The links involving K248 in the 2nd Triad are lost in the closed state.

The only "new" interacting pair in the closed state is the following:
i-pr = 3 pair is A 64 LYS A 66 TYR coupling-energy = 8.31 kT
but it is not well conserved in other pLGIC bacterial sequences.
Interestingly, most of the "lost/gained" interactions involve either Loop C or the ECD-TMD interface (Cys-Loop, pre-M1, M2-M3 loop)
We note that in the closed state the R192-D122 and R192-D32 electrostatics interactions are lowered to about 6 kT each.

11.2 pKa calculation for Asp and Glu using FD/DH for all subunits

We show below the complete table of calculated pKas for Aspartates and Glutamates: O-1 to O-5 and C-1 to C-5 represent pKas for each subunit (1 to 5) for the open form and the closed form, respectively; then the average and the rmsd is presented, and finally the difference between the two forms.

Res	O-1	O-2	O-3	O-4	O-5	C-1	C-2	C-3	C-4	C-5	O	Rms	C	Rms	Diff
D13	3.78	3.37	3.64	3.67	3.25	4.25	3.75	4.24	4.24	3.80	3.54	0.20	4.06	0.23	-0.51
E14	3.03	3.64	1.87	2.97	3.11	2.67	3.75	2.67	2.19	2.63	2.92	0.58	2.78	0.52	0.14
E26	7.07	6.43	7.03	6.66	7.30	7.77	4.74	3.77	6.25	5.23	**6.90**	0.31	**5.55**	1.37	1.35
D31	2.75	1.73	2.04	1.67	2.77	1.98	2.19	1.37	2.06	1.14	2.19	0.48	1.75	0.41	0.44
D32	2.25	2.22	1.33	2.27	1.49	2.46	3.24	3.17	2.33	3.36	1.91	0.41	2.91	0.43	-1.00
E35	4.98	5.37	6.05	6.09	5.81	4.74	4.26	4.25	4.74	4.26	**5.66**	0.43	4.45	0.24	1.21
D49	3.78	3.81	4.75	5.03	4.73	4.27	6.57	3.78	5.21	4.25	4.42	0.52	4.82	0.99	-0.40
D55	2.42	3.75	2.34	2.34	3.08	4.24	4.21	2.99	3.64	3.26	2.79	0.56	3.67	0.50	-0.88
E67	5.22	5.71	3.87	4.69	4.34	5.74	3.37	4.77	4.75	5.25	4.77	0.65	4.78	0.79	-0.01
E69	3.38	4.68	5.11	4.43	3.38	3.37	4.75	3.67	3.76	4.27	4.20	0.70	3.96	0.49	0.23
E75	4.89	3.80	5.14	4.60	3.78	3.14	3.77	3.66	3.73	2.87	4.44	0.56	3.43	0.36	1.01
E82	3.63	2.34	4.28	3.22	2.33	2.76	3.23	2.42	3.02	2.89	3.16	0.75	2.86	0.27	0.30
D86	2.61	2.36	4.12	3.09	3.78	2.88	3.63	3.75	2.76	2.24	3.19	0.67	3.05	0.56	0.14
D88	1.44	2.78	2.77	1.38	2.16	2.78	3.75	2.46	2.34	2.81	2.11	0.61	2.83	0.50	-0.72
D91	2.23	2.71	3.20	2.30	2.29	2.47	3.12	2.81	3.28	3.64	2.55	0.37	3.06	0.40	-0.52
D97	2.74	2.70	1.64	2.68	1.35	2.23	2.77	2.26	2.64	2.85	2.22	0.60	2.55	0.26	-0.33
E104	1.87	4.45	3.29	5.05	3.80	5.75	5.75	7.26	4.26	3.77	3.69	1.09	**5.36**	1.24	-1.67
D115	3.16	2.85	3.13	3.11	2.86	2.82	2.70	3.24	3.15	2.82	3.02	0.14	2.95	0.21	0.08
D122	0.03	0.22	0.17	0.19	-0.1	1.63	0.01	1.10	5.77	4.75	0.10	0.12	2.65	2.22	-2.55
D136	3.13	4.10	3.71	3.11	3.22	3.13	2.88	4.23	3.18	3.37	3.45	0.39	3.36	0.46	0.10
D145	3.23	3.75	3.31	4.27	3.20	3.25	3.03	6.34	4.24	2.88	3.55	0.41	3.95	1.29	-0.40
E147	4.31	3.26	4.44	4.59	5.02	4.75	4.74	5.25	4.25	3.37	4.32	0.58	4.47	0.64	-0.15
D153	3.25	3.35	3.63	3.77	3.64	4.73	3.77	4.24	3.76	3.38	3.53	0.20	3.98	0.47	-0.45
D154	3.75	3.67	3.12	4.21	3.35	3.24	4.76	3.62	1.42	4.23	3.62	0.37	3.45	1.14	0.17
D161	4.27	3.64	3.67	3.36	3.76	3.66	3.76	3.67	3.76	3.76	3.74	0.30	3.72	0.05	0.02
E163	4.23	4.39	3.37	3.80	4.56	5.23	3.26	4.74	3.75	3.36	4.07	0.43	4.07	0.78	0.00
E177	5.83	7.22	4.25	6.91	3.76	4.78	5.24	4.75	5.75	3.39	**5.59**	1.39	4.78	0.79	0.81
D178	2.93	2.94	2.95	3.77	2.99	3.75	3.75	3.25	3.37	3.74	3.12	0.33	3.57	0.22	-0.46
E181	2.15	0.84	1.45	1.25	1.61	4.25	3.25	3.27	4.55	3.36	1.46	0.43	3.74	0.55	-2.28
D185	1.79	1.70	2.13	2.16	1.60	1.38	1.42	0.97	2.39	0.98	1.88	0.23	1.43	0.52	0.45
E222	1.47	2.30	1.82	2.24	3.63	2.74	2.49	1.39	2.41	3.75	2.29	0.73	2.56	0.75	-0.26
E243	4.30	4.73	3.81	4.23	3.38	4.26	3.76	4.74	3.78	3.28	4.09	0.46	3.96	0.50	0.13
E272	4.40	3.38	3.66	4.28	3.76	3.66	3.37	3.37	3.76	3.37	3.90	0.39	3.51	0.17	0.39
E282	4.47	4.35	4.56	4.30	4.24	4.24	4.24	4.23	4.24	3.76	4.38	0.12	4.14	0.19	0.24

We have underlined those values that have a high rmsd and put in bold those pKas that are above 5, suggesting that these residues might play a role during the pH-driven transition ($pH_{50} = 5.2$).

The residues that have $|\Delta pKa| > 1$ are: 104 and 181 (we omit 32 and 122 which cannot be studied by mutagenesis), and 26, 35, 75 and 177.
We note that we could also calculate a normalized difference of pKa ($\Delta pKa/\sigma_{tot}$) where ($\sigma^2_{tot} = \sigma^2_O + \sigma^2_C$). In this case, E35 and E181 would be the main ones to stand out.

Supplementary Materials and methods

Structure-based pKa calculations by the FD-DH method

The original Fortran code from J. Warwicker[1] was adapted to enable the handling of larger protein assemblies such as the GLIC pentamer. Default values for all the parameters were adopted: the salt concentration is set to 0.15 M NaCl and the dielectric constant is taken to be 4 inside the protein and 78 in the bulk solvent. No special treatment was used to model the membrane, as it was shown for two membrane proteins to have little effects on the results[2]. The reported pKa values are the mean values averaged over the five monomers (**SI Appendix, Notes**).

Protein expression and purification

Purification of GLIC mutants followed the same procedure as previously reported[3]. Briefly, plasmids containing the N-terminal GLIC gene fused with the Maltose Binding Protein (MBP) gene were transformed into *E. coli* C43 cell lines. The cells were cultured in 2YT medium in presence of 100 mg/ml Ampicillin and were incubated at 37°. 0.1-0.2 mM of IPTG was added into the medium when the OD reached 0.8-1.0, followed by a decrease of the incubation temperature to 20°. GLIC was extracted from *E. coli* membrane with buffer A containing 300 mM NaCl, 20 mM Tris pH 7.6, and 2% DDM. Solubilized proteins were loaded onto an amylose-binding resin, which was pre-equilibrated with buffer A, and incubated around 30-40 minutes. Amylose-binding resin was washed with buffer A containing 0.1% DDM and then washed with buffer A containing 0.02% DDM. The MBP tag was cut off by incubating recombinant MBP-GLIC bound resin with thrombin enzyme overnight. The elution-containing GLIC was further purified by size-exclusion chromatography (Superose 6 10/300) with buffer A containing 0.02% DDM. The fraction with the peak corresponding to GLIC pentamer was collected and concentrated to 8-10 mg/ml and the protein was flash frozen using liquid nitrogen and then stored at -80° for further use.

Reconstitution of GLIC in lipids

0.2 mg of detergent solubilized GLIC was added in 100 μl buffer solution (150 mM NaCl, 20 mM Tris, 0.02 % DDM, pH 7.6) containing a 5:2 mixture (w:w) of 0.5 mg POPE/POPG, and stored at 4°C for 3 hours. We initially screened several conditions for the reconstitution of GLIC in lipids, until we found conditions that give a titration curve for the wild-type with the same pH50 than other functional studies. We then settled for these conditions throughout our FT-IR studies. The molar ratio of GLIC:lipid was about 1:120. 10 mg of BioBeads were added to the solution and incubated overnight. Subsequently, BioBeads were removed and the solution was centrifuged twice at 15.000 rpm for 15 mins. After the supernatant was removed, the sediment was resuspended in 100 μl of 20 mM Tris-HCl buffer (pH 7.6). The final concentration of the reconstituted GLIC was about 6 mg/ml.

pH titrations by ATR-FTIR measurements

10 μl of freshly lipid reconstituted GLIC was added on the surface of the diamond reflection element of the ATR unit. The buffer solvent of the sample solution was evaporated under an argon stream. Subsequently, the sample was immersed in 8 ml of a buffer solution (150 mM NaCl, 20 mM HEPES, 20 mM MES, pH = 8.3). Under these conditions the protein-lipid film remains adhered to the surface of the internal reflection element. After the re-hydration process reached completion (> 30 minutes), a 512 reference spectrum were co-added at pH 8.3. For studies of the channel opening process, 2 to 20 μl of 1 M HCl solution were added to the sample solution and stirred with the help of the pipette. The addition of HCl typically lead to a drop by 0.2 to 0.4 pH units and the final pH was checked by a glass electrode directly mounted to the ATR cell (**SI Appendix, Fig. S1**) After pH equilibration, a 512 sample spectra were recorded. A set of difference spectra was collected at various pH values by repeating the former procedure until the pH reached 2.0.

Band assignment of the pH-induced different FT-IR spectra

The bands observed in the pH induced different spectra shown in **Fig. 2** consist of contributions not only from the protein but also from different background species such as the lipid bilayer and the buffer solution. For the analysis of the

spectral data, the bands have to be appropriately assigned to each species. **SI Appendix, Fig. S1B-E** shows a comparison of FTIR spectra for all reference samples. The spectrum of GLIC reconstituted in the POPE/POPG lipid mixture is shown in **SI Appendix, Fig. S1B**, while the spectrum of sole POPE/POPC lipid bilayer is shown in **SI Appendix, Fig. S1C** (both in semi-dry states). Comparison of the two spectra enables us to assign the bands at 1653 (α-helical, amide I), 1636 (β-sheet, amide I), 1539 (amide II), 1520 (amide II), 1404 (amide III) cm^{-1} to the protein. **SI Appendix, Fig. S1D** shows the pH-induced FTIR difference spectra of the HEPES/MES buffer solution in the absence of lipid or protein, which highlights the contribution of the buffer bands in the pH induced difference spectra of the lipid reconstituted GLIC in **SI Appendix, Fig. S1E**. Finally, the bands that can be uniquely assigned to the protein during the pH change are those at 1718, 1657, 1628, 1574, 1537, 1520, 1400 cm-1 (indicated with * in **SI Appendix, Fig. S1E**).

Normalization of $\nu_s(COO^-)$ band intensities for the FT-IR spectra

Despite the fact that all samples were prepared under equivalent conditions, the spectra show slightly different intensities for each band because of differences in protein concentration, slight differences of the lipid/protein ratio, and instability due to swelling of the membrane. In order to compare these different data sets, intensity normalization was performed for each of the bands in the spectra. The $\nu_s(COO^-)$ band at 1400 cm^{-1} was chosen for the analysis of the protonation state of the carboxyl groups in Glu or Asp groups. Peak height differences between 1400 cm^{-1} and 1417 cm^{-1}, where the former represents peak position and the latter represents the bottom edge of the peak as a baseline, were taken at every measured pH from each data set as measures of the relative contents of deprotonated carboxyl groups. The peak height differences without any normalization are shown in the **SI Appendix, Fig. S3A**. Because of differences in the experimental conditions, the intensities varied from -0.005 to -0.011 (~ 45 %) at pH = 2 for different samples. For normalization of these intensities, we introduced the following assumptions. First, we assumed that all carboxyl groups in the proteins are protonated at pH = 2. Although the curves in **SI Appendix, Fig. S3A** does not saturate at pH = 2, which is partially due to instability of the lipid layer against the acidic solution environment, we made the assumption that the majority of the carboxylic groups were all protonated, such that the

normalization factor was set to one at this pH. Then, the second assumption is that the normalization factor at pH = 2 for those mutations that replaced Glu or Asp to other non-carboxylic amino acids was set to 0.97. Wild-type GLIC contains a total of 35 carboxyl groups comprising 19 Asp and 16 Glu residues. Therefore, the carboxyl intensities of the mutants should be (35-1)/35 = 0.97. This assumption is based on the idea that there are no significant differences among the absorption coefficients of each carboxyl group. The plot of the normalized carboxylic band intensities vs pH is shown in **SI Appendix, Fig. S3B**. Comparison of the pH titration curves for each mutant was made on the basis of these normalized traces. The interpretation of the pH titration difference spectra for mutants is described in **SI Appendix, Notes**.

Protein crystallization and structure determination.

All of the crystals were grown with the hanging drop evaporation method at 18°. 1 µl protein was mixed with 1 µl buffer containing 12%-14% PEG 4000, 400 mM NaSCN, 16% glycerol, 3% DMSO and 0.1 M NaAcetate pH 4 against 1 ml of mother liquor. In order to improve the quality and reproducibility of crystals, the micro-seeding procedure was performed after setting up crystallization. The crystals were flash frozen using liquid nitrogen directly. The diffraction images were collected either at ESRF (European Synchrotron Radiation Facility, beamlines ID30, ID29, and ID23) or Synchrotron-Soleil (beamlines PX1 and PX2). The data sets were indexed and analyzed by the software xdsme[4] and further processed by CCP4 programs. The phase problem was solved by molecular replacement using Molrep[5]. Further refinements of the models were performed using Refmac refinement[5] alternated with manual building in COOT[6]. The qualities of the final structure models were checked by Molprobity webserver[7]. The figures showing structural models were prepared using Chimera[8]. The HOLE software[9] was used to analyze the channel diameter.

Electrophysiological recordings

Functional recordings of GLIC were done on *Xenopus* oocytes provided by the Centre de Ressources Biologiques Xénopes–Rennes (France). Oocytes were stored in MBS buffer (88 mM NaCl, 1 mM KCl, 2.5 mM $NaHCO_3$, 0.7 mM $CaCl_2$, 1 mM $MgSO_4$, and 5 mM HEPES pH 7.4) and functional recordings were made in MES

buffer (100 mM NaCl, 3 mM KCl, 1 mM $CaCl_2$, 1 mM $MgCl_2$ and 10 mM MES pH 7.4) equilibrated at the appropriate pHs using 1 M HCl. Two-electrode voltage clamp recordings were performed at -40 mV, after allowing 48–96 hr for GLIC or mutants expression, as previously described[10]. Mutants leading to currents smaller than 500 nA at high proton concentrations (pH 4) were categorized as non-functional. Electrophysiological recordings were analyzed using AxoGraph X and ClampFit (Molecular Devices, Sunnyvale, CA). The Hill equation was used for the dose-response fits to determine the pH_{50}, EC_{50} and nH values for each construct:

$$y(x) = \frac{a * x^{nH}}{x^{nH} + {EC_{50}}^{nH}}$$

where a represents the maximal current value after normalization, nH represents the Hill number and EC_{50} the proton concentration for which half of the maximal electrophysiological response is recorded.

MTS derivatives (Aldrich Chemical Co) were dissolved from stock solutions in recording buffer prior to each experiment without exceeding 0.1% of final DMSO concentration. DTT (Sigma) and Picrotoxinin (Sigma) were directly dissolved at the appropriate concentration in recording buffer. Solutions were made fresh each day prior to functional recordings.

Xenopus oocytes immunolabeling

Xenopus oocytes were nucleus-injected with a mix of two pmt3 vectors, one containing mutant-GLIC-HA cDNA (80 ng/μl), the other containing GFP (10 ng/μl). Control oocytes were injected with GFP alone or a mix of WT-GLIC-HA and GFP vectors. After 96 h of protein expression, GFP positive cells were fixed in 4% paraformaldehyde (4˚C, O/N), blocked in PBS + 4% horse serum (30 min, RT (Sigma Aldrich)), and immunolabeled in PBS + 2% horse serum with a rabbit anti-HA primary antibody (1.5 h, RT) and an anti-rabbit Cy5 coupled secondary antibody (1 h, RT (ThermoFisher Scientific)). Follow immunolabeling, oocytes were fixed again in 4% paraformaldehyde (4˚C, O/N), imbedded into 3% low-melting agarose blocks, and sliced at 40 μm intervals. Slices were mounted on glass slides and imaged using epi-fluorescence microscopy with constant exposure times.

Reference

[1] J. Warwicker, ‘Improved pKa calculations through flexibility based sampling of a water-dominated interaction scheme’, *Protein Sci. Publ. Protein Soc.*, vol. 13, no. 10, pp. 2793–2805, Oct. 2004.
[2] I. Sazanavets and J. Warwicker, ‘Computational Tools for Interpreting Ion Channel pH-Dependence’, *PloS One*, vol. 10, no. 4, p. e0125293, 2015.
[3] N. Bocquet *et al.*, ‘X-ray structure of a pentameric ligand-gated ion channel in an apparently open conformation’, *Nature*, vol. 457, no. 7225, pp. 111–114, 2009.
[4] ‘Google Code Archive - Long-term storage for Google Code Project Hosting.’ [Online]. Available: https://code.google.com/archive/p/xdsme/. [Accessed: 10-May-2017].
[5] Collaborative Computational Project, Number 4, ‘The CCP4 suite: programs for protein crystallography’, *Acta Crystallogr. D Biol. Crystallogr.*, vol. 50, no. Pt 5, pp. 760–763, Sep. 1994.
[6] P. Emsley, B. Lohkamp, W. G. Scott, and K. Cowtan, ‘Features and development of Coot’, *Acta Crystallogr. D Biol. Crystallogr.*, vol. 66, no. 4, pp. 486–501, Apr. 2010.
[7] V. B. Chen *et al.*, ‘MolProbity: all-atom structure validation for macromolecular crystallography’, *Acta Crystallogr. D Biol. Crystallogr.*, vol. 66, no. Pt 1, pp. 12–21, Jan. 2010.
[8] E. F. Pettersen *et al.*, ‘UCSF Chimera--a visualization system for exploratory research and analysis’, *J. Comput. Chem.*, vol. 25, no. 13, pp. 1605–1612, Oct. 2004.
[9] O. S. Smart, J. G. Neduvelil, X. Wang, B. A. Wallace, and M. S. Sansom, ‘HOLE: a program for the analysis of the pore dimensions of ion channel structural models’, *J. Mol. Graph.*, vol. 14, no. 6, pp. 354–360, 376, Dec. 1996.
[10] G. Duret *et al.*, ‘Functional prokaryotic-eukaryotic chimera from the pentameric ligand-gated ion channel family’, *Proc. Natl. Acad. Sci. U. S. A.*, vol. 108, no. 29, pp. 12143–12148, Jul. 2011.